Copper Access Networks for Wireline and Wireless Services

Eduardo Lins de Medeiros

LUND UNIVERSITY

Licentiate Thesis
Electrical Engineering
Lund, November 2015

Eduardo Lins de Medeiros
Department of Electrical and Information Technology
Electrical Engineering
Lund University
P.O. Box 118, 221 00 Lund, Sweden

Series of licentiate and doctoral dissertations
ISSN 1654-790X; No. 77
ISBN 978-91-7623-534-8 (print)
ISBN 978-91-7623-535-5 (pdf)

Typeset in Palatino and Helvetica using LaTeX 2_ε.
Printed in Sweden by Tryckeriet i E-huset, Lund University, Lund.

To Alina

Abstract

In the last few years, technologies for broadband delivery over copper have dealt with increased capacity demands by using high frequencies and transmitter coordination, also known as vectoring. At the same time, to provide high capacity mobile broadband, operators have resorted to small cells. The work compiled into this dissertation covers both vectoring in traditional and future wireline services as the use of copper access infrastructure to deploy high capacity small cells.

In the first part of this dissertation, chapters 2 to 5, we investigate issues with vectoring deployment, namely side effects of impedance changes and its consequences for the stability and performance of vectoring bundles.

In the second part of this dissertation, chapters 6 and 7, we investigate the feasibility of using the copper access network infrastructure to offer mobile broadband services via co-deployment of Digital Subscriber Line (DSL) and Long Term Evolution (LTE) equipment. The proposed architecture is based on analog transmission of the radio signal at frequencies adequate to the copper medium.

Contents

Preface

This dissertation consists of an introduction, followed by a compilation of five conference papers and journal paper.

- Driton Statovci, Thomas Magesacher, Martin Wolkerstorfer, and Eduardo Medeiros, »Analysis of Fast Initialization for Vectored Wireline Systems«, *IEEE Global Telecommunications Conference (GLOBECOM)*, Dec 2013.
- Eduardo Medeiros, Thomas Magesacher, Per-Erik Eriksson, Chenguang Lu, and Per Ödling, »How Vectoring in G.fast May Cause Neighborhood Wars«, *IEEE International Conference on Communications (ICC)*, Jun 2014.
- Eduardo Medeiros, Thomas Magesacher, Per Ödling, Dong Wei, Xiang Wang, Qiaojie Li, Per-Erik Eriksson, Chenguang Lu, Jeroen Boschma, and Bas van den Heuvel, »Modeling Alien-Line Impedance Mismatch in Wideband Vectored Wireline Systems«, *IEEE Communications Letters*, Sep 2014, vol. 18, number 9.
- Yezi Huang, Thomas Magesacher, Eduardo Medeiros, Per-Erik Eriksson, Chenguang Lu, and Per Ödling, »Mitigating Disorderly Leaving Events in G.fast«, *IEEE International Conference on Communications (ICC)*, Jun 2015.
- Yezi Huang, Eduardo Medeiros, Stefan Höst, Thomas Magesacher, Per-Erik Eriksson, Chenguang Lu, Per Ödling and Per Ola Börjesson, »Enabling DSL and Radio on the Same Copper Pair«, *IEEE International Conference on Communications (ICC)*, Jun 2015.
- Yezi Huang, Eduardo Medeiros, Stefan Höst, Thomas Magesacher, Per-Erik Eriksson, Chenguang Lu, Per Ödling and Per Ola Börjesson, »LTE Over Copper - Potential and Limitations«, *IEEE International Symposium on Personal, Indoor and Mobile Radio Communications - (PIMRC)*, Sep 2015.

Acknowledgments

This licentiate dissertation was conceived in a special and unique setting, at the confluence of industry and academia in Kista, where LTH shares office and laboratory space with Ericsson AB. As such, it positioned me to work on practical, relevant research questions, while having access to a group of world-leading experts to which I'm most indebted. I specially would like to thank the Small Cell Transport team led by Henrik Almeida, namely my colleagues and co-authors Pelle, Chenguang, Boris, Daniel, Elmar, Gemma, Keke, Miguel, and Patryk. Also at Ericsson I would like to thank Kåre Gustafsson, the Multipurpose Transport team and Sándor Albrecht.

Another focus of my gratitude goes to the group of industry and academia experts reunited under the GOLD consortium. During the first years in this licentiate they provided a very diverse and interesting forum for discussion of ideas, always providing thorough and constructive feedback. Thanks to Martin, Torsten, Jochen, Anas, Trevor, Les, Marcos, Hubert, Orem, Marta, José, Enrique, Rob, Bas, Antoni, Kaan, Jens and Ian, the latter also a co-founder of the "dangerous lunches club" in Kista.

I was fortunate to collaborate with Driton, Martin and Sanda, from FTW/TU Wien, Bas van den Heuvel and Jeroen Boschma from TNO, Dong Wei, Xiang Wang and Qiaojie Li from Huawei and Nilma Fonseca from UFPA. It is an honor to have them as co-authors on some of the papers compiled into this dissertation.

I dedicate a paragraph to my colleague and co-author Yezi Huang. Yezi is extra talented, dedicated and quick. I foresee that many lines will still be written about her, but remember that you read it here first!

Maturing as a researcher is a long and demanding process. Lund's Broadband Research group helps immensely by providing a wealth of the most important resource: accessible role models. In this category I would like to ac-

knowledge Per Ola Börjesson, Thomas Magesacher, Stefan Höst and Pernilla Schuber.

Much could be said about the talents of my supervisor, Per Ödling. One could praise his original problem solving skills, his charisma or his excellent apple jack. Instead I chose to remark in print that he is »cool«. I also thank his better half Gisela, for being a most gracious host and making me feel at home, away from home.

Mentioning home, I thank my family who always stimulated and invested in my education. I also thank Aldebaro Klautau who a long time ago told me what a modern engineer should be like.

Special thanks are reserved to my lovely wife and muse Alina. She is a source of inspiration and encouragement at all times.

Finally I acknowledge the support of Celtic-Plus and Vinnova - the Swedish Governmental Agency for Innovation Systems through the HFCC/G.fast and GOLD projects. The work compiled into this dissertation has also been supported by EIT Digital and the European Horizon 2020 project Xhaul.

Eduardo
Stockholm, November 2015

1

Introduction

For years Digital Subscriber Line (DSL) services have been used to provide stable, moderately high capacity connections for homes. To deal with increased capacity demands, DSL standards have evolved by increasing the bandwidth and adopting synchronized transmission over multiple lines together with crosstalk cancellation techniques known as vectoring. Concurrently, in the last few years the mobile industry has shifted from providing good quality voice services to provide decent mobile broadband connections, paving the way to the ubiquitous smartphone and tablets.

The contributions compiled in this dissertation parallel the telecom industry shift from providing high speed wireline services to offering wireline wireless service bundles over their legacy copper plant infrastructure. This shift in industry is reflected in the two parts this thesis is divided.

Part I comprises of chapters 2 to 5 and covers VDSL2 vectoring initialization improvements as well as a treatment of impedance mismatch effects over vectoring performance. A brief description of each chapter is presented next.

- In Chapter 2, consisting of the conference paper **Analysis of Fast Initialization for Vectored Wireline Systems**, originally published in *Proc. IEEE Global Communications Conference (GLOBECOM 2013)*, we present an alternative fast initialization method for vectored VDSL2, that takes advantage of previously stored channel coefficients.

- Chapter 3 consists of the conference paper **How Vectoring in G.fast May Cause Neighborhood Wars**, originally Published in *Proc. IEEE International Conference on Communications (ICC 2014)*. In this contribution we present measurements that confirm the impact of impedance changes in lines neighboring an active G.fast vectored group. We also

evaluate the feasibility of a decision-directed channel tracking procedure to alleviate the problem.

- Chapter 4 consists of the letter **Modeling Alien-Line Impedance-Mismatch in Wideband Vectored Wireline Systems**, originally published in *IEEE Communications Letters*, vol. 18, no. 9, September 2014. This letter presents a model for the effect of impedance changes in vectored groups. The model is validated with measurements and explains the results observed in Chapter 3.

- Chapter 5 consists of the conference paper **Mitigating Disorderly Leaving Events in G.fast**, originally published in *Proc. IEEE International Conference on Communications (ICC 2015)*. In this paper we use the model developed in the previous contribution to explain the large SNR loss caused by disorderly leaving events in G.fast. A fast and efficient precoder update procedure is proposed to avoid SNR loss due to modems leaving a vectored group.

Part II of this dissertation proposes a new use for operator's copper plants as a means to deliver a complementary wireless service capability. In chapters 6 and 7 we propose a centralized baseband architecture for deploying modern OFDM-based wireless signals over copper in analog form. A brief description of each chapter is provided next.

- Chapter 6 consists of the conference paper **Enabling DSL and Radio on the Same Copper Pair** *Proc. IEEE International Conference on Communications (ICC 2015)*. In this paper we discuss an analog radio over copper system, taking advantage of the frequency bands between VDSL2 and G.fast. We investigate efficient band plans and rate-reach curves for such a system.

- Chapter 7 consists of the conference paper **LTE Over Copper - Potential and Limitations** Published in *Proc. IEEE Symposium on Personal, Indoor and Mobile Radio Communications - (PIMRC)*. In this paper we go further on the analysis of the radio over copper system, by investigating the trade-offs imposed by 3GPP compliancy.

2

Analysis of Fast Initialization for Vectored Wireline Systems

Driton Statovci, Thomas Magesacher, Martin Wolkerstorfer, and Eduardo Medeiros

Abstract

Cooperation of transceivers on signal level at the remote terminal—often referred to as vectoring—is an effective approach to mitigate crosstalk in wireline transmission systems. While the gain in bitrate compared to crosstalk-limited transmission is substantial, the initialization of a vectoring system requires time and care to ensure system stability. In this contribution, a fast initialization scheme for vectored wireline systems based on spectral protection is analyzed. Two scenarios are considered, where in the first one no prior channel information is available, and in the second one erroneous prior knowledge of channel coefficients is utilized. Measurements on a commercial VDSL2 vectoring platform and throughput simulations demonstrate the potential of the fast initialization scheme.[1]

[1]Published in *Proc. IEEE Global Communications Conference (GLOBECOM 2013)*, Atlanta, USA, 9-13 Dec. 2013.

2.1 INTRODUCTION

In modern wireline transmission systems, co-location of transceivers at the remote terminal allows for coordination with the aim of better exploiting the potential of the cable through techniques summarized under the term dynamic spectrum management (DSM) [1]. The degree of coordination ranges from single-line power control (DSM level 1) over multi-line power-spectrum control (DSM level 2) to joint signal processing (DSM level 3). Methods for joint processing of transmit signals (pre-coding) and joint processing of receive signals (interference cancellation) are often summarized under the term vectoring or vectored transmission [2–8]. Network operators have used DSM level 1 and level 2 to improve the performance and stability of their systems. Recently they have started deploying vectored systems (DSM level 3) mainly from street cabinets aiming at increasing bitrates [9].

Vectoring has the potential to turn crosstalk-limited systems into background-noise-limited systems, which can yield substantial gains in bitrate [10]. A prerequisite for well-working precoders and cancelers are accurate channel estimates, which are obtained in the initialization phase and continuously updated during the showtime phase. State-of-the-art initialization procedures (such as the very high speed digital subscriber line 2 (VDSL2) initialization defined in the standard G.993.5 [11]) can take up to several minutes until joining users experience connectivity. The protection of vectored lines against joining, initializing lines has been a prominent issue in standardization. Corresponding approaches include for instance the reuse of previously collected channel information, or the limitation of the received crosstalk noise to a well-defined level below the noise margin [12] [13]. In [14] a channel estimation technique based on the signal-to-noise ratio (SNR) is proposed, where the transmit power limitation of the initializing disturber line is gradually loosened as the channel estimate becomes more accurate.

In this paper, we revisit the ideas of using outdated channel information and spectral protection of vectored lines, and merge them into a fast-initialization scheme conform with the G.993.5 standard. Furthermore, we analyze the available bitrate of the *joining* lines when the crosstalk noise limitation imposed by vectored lines is based on one of two assumptions: a) based on empirical worst-case channels in case of no channel knowledge; or b) based on outdated channel information and an estimated channel error variance. The performance analysis under erroneous channel coefficients is based on [15], where zero forcing (ZF) and diagonalizing precoding (DP) were considered as vectoring algorithms. In [16] the effect of *direct channel* estimation errors in a crosstalk-free setting is analyzed. Similarly as in [16] we consider an estimation error variance that is normalized by the corresponding channel gain. Despite likely dependencies of the estimation error on the SNR [16], we

assume a frequency-flat normalized error in our numerical examples in order to avoid dependence on a specific channel estimation method. Furthermore, as in [14] [15] we assume that the direct channels are estimated correctly and consider normalized crosstalk channel errors only.

The paper is organized as follows. In Section 2.2 and Section 2.3, the vectoring initialization phase is described and analyzed, respectively. In Section 2.4, measurements of vectored VDSL2 channels over time are presented and the time variation is quantified. Simulation results of an access scenario with tree-type topology and 15 users are presented in Section 2.5. Finally, Section 2.6 concludes the work.

2.2 SPECTRAL PROTECTION FOR FAST INITIALIZATION

A typical initialization procedure, illustrated in Figure 2.1, consists of channel estimation (channel discovery phase), adaptation of receiver parameters to the channel (training phase), and computation as well as exchange of bitloading tables (channel analysis and exchange phase) [10]. Initialization of vectored systems requires additional phases and is typically done in two steps: first, the crosstalk from joining lines into vectored lines is estimated and compensated; second, the joining lines estimate and compensate crosstalk from vectored lines. The VDSL2 standard G.993.5 refers to these phases as "VECTOR-1" and "VECTOR-2", respectively [11].

In the following we analyze the spectral protection of vectored VDSL2 lines from initializing lines, thereby ensuring network stability, under two cases of prior channel knowledge. Without loss of generality we assume that only one new user at a time is joining the vectoring group.

Case 1: The new user has no channel information from previous showtime-occasions but knows the worst-case far-end crosstalk (FEXT) coupling magnitude into other users' lines—a parameter that can be estimated based on models and some knowledge of the network topology, such as loop length and cable type. Based on this worst-case FEXT coupling magnitude, the new user determines its transmit power spectral density (PSD) such that the noise increase seen by users in the vectoring group does not exceed a factor q, where $q \geq 1$ is chosen such that the SNR decay[2] remains well below the SNR margin (e.g., $10 \log_{10} q < 2\,\mathrm{dB}$). As soon as the transmit-PSD computation is finished, the new user starts to transmit without joining and without disturbing the vectoring group ("controlled alien"). Although the new user might achieve only a modest bitrate, it can transmit and receive immediately which yields

[2]For simplicity, we use the term "noise" for background noise, alien interference, and residual interference caused by users in the vectoring group with imperfect channel knowledge.

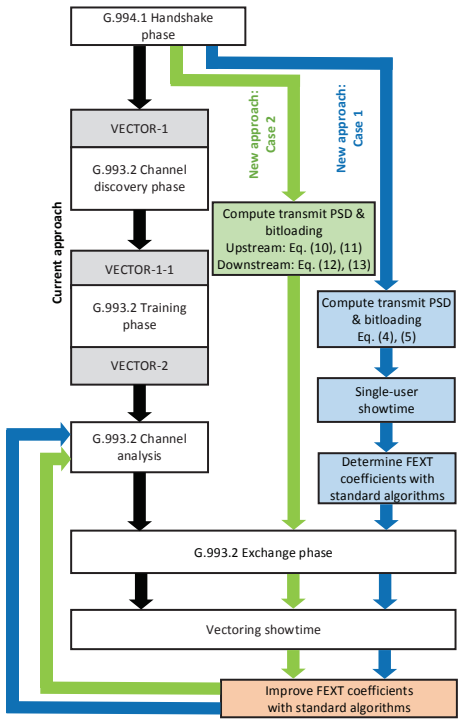

Figure 2.1: Illustration of initialization in vectored VDSL2 systems: Current approach and extensions for Case 1 and Case 2.

an improved connectivity-experience for the customer. While operating as a controlled alien, the new user gathers vector-channel information before eventually joining the vectoring group following state-of-the-art procedures (cf. Figure 2.1).

Case 2: The new user knows the "old" complex coupling coefficients from a previous showtime occasion and their error variances. The error variances could, for example, be estimated based on the time variance of the coefficients observed in the vectoring group. Based on this knowledge, the new user determines its transmit PSD such that the SNR-margin decay of the lines in the vectoring group is kept below q. As soon as the transmit-PSD computation is finished, the new user joins the vectoring group and starts to transmit.

Clearly, partial or inaccurate channel knowledge will result in suboptimal bitrates, analyzed in Section 2.3, for the new user. The benefit of fast initialization is improved user experience through immediate connectivity. The stability of the vectoring system is ensured. Immediately after starting to transmit, the new user begins to gather (Case 1) or improve (Case 2) its vector

channel information in order to reach its maximum bitrate as soon as possible.

2.3 ANALYSIS

We consider a vectoring system with U users denoted by the set $\mathcal{U} = \{1, \ldots, k-1, k, k+1, \ldots, U\}$, where k denotes the new user and all other users are part of the vectoring group. For simplicity, the analysis is limited to linear vectoring systems that use a ZF canceler [7] and a DP [8] for upstream and downstream transmission, respectively.

2.3.1 CASE 1

The FEXT magnitudes of the new line k into the vectored lines can be estimated based on worst-case FEXT coupling models or FEXT models of a particular network operator, knowledge of direct channels, and line lengths. Since the line k is not part of the vectoring group, transmission on line k will increase the level of noise on all vectored lines. The increased noise level on line u and tone c is given by

$$\hat{\sigma}_u^c = \sigma_u^c + \left|[\mathbf{H}_{\text{est}}^c]_{uk}\right|^2 p_k^c, \tag{2.1}$$

where p_k^c is the transmit PSD of user k, σ_u denotes the PSD of the background noise, and $[\mathbf{H}_{\text{est}}^c]_{uk}$ denotes the estimated FEXT channel transfer function from user k to user u. For each tone, we want to protect the user that is disturbed most by the joining user k. For this purpose we define the magnitude of the worst-case FEXT coupling

$$|h_{\text{WC}}^c| = \max_{u \in \mathcal{U} \setminus k} \left|[\mathbf{H}_{\text{est}}^c]_{uk}\right|. \tag{2.2}$$

In order to ensure stability of the vectoring system, we introduce the parameter $q \geq 1$, which controls the maximum noise level any vectored line is experiencing:

$$\hat{\sigma}_u^c \leq q\sigma_u^c. \tag{2.3}$$

With (2.1), (2.2) and (2.3), the maximum transmit PSD of user k is given by

$$p_k^{c,\max} = \min_{u \in \mathcal{U} \setminus k} \frac{\sigma_u^c (q-1)}{\left|h_{\text{WC}}^c\right|^2}. \tag{2.4}$$

The maximum number of bits user k is able to transmit on tone c is calculated by

$$r_k^c = \log_2 \left(1 + \frac{\left|[\mathbf{H}_{\text{est}}^c]_{kk}\right|^2 \min\left(p_k^{c,\max}, p_k^{c,\text{mask}}\right)}{\Gamma\left(\sum_{j \in \mathcal{U} \setminus k} \left|[\mathbf{H}_{\text{est}}^c]_{kj}\right|^2 p_j^c + \sigma_k^c\right)} \right), \tag{2.5}$$

where Γ is the SNR gap to capacity and $p_k^{c,\text{mask}}$ is the PSD mask level on tone c, which is usually selected to be the same for all lines.

Note that the vectored lines will maintain their bitrate. Since DSL systems operate with a noise margin of at least 6 dB, an increase of the total noise on a particular line[3] by, for example, $q = 1.58$ (2 dB) until the system has learned the channel coefficients of line k should have no impact on bitrate.

2.3.2 CASE 2

We assume that both magnitude and phase of the FEXT coupling coefficients of line k from and into vectored lines are partially known. For example, the coefficients from the last time line k was part of the vectoring group can be used. In the following, we analyze ZF and DP for upstream and downstream transmission directions, respectively.

Upstream: Based on the derivation in [15], the noise variance seen by user u on tone c at the output of the ZF canceler under imperfect channel estimation can be calculated as

$$\hat{\sigma}_{u,\text{ZF}}^c = \underbrace{\sum_{i,j\in\mathcal{U}} \left|[\mathbf{G}^c]_{ui}\right|^2 \delta_{ij}^c p_j^c}_{\text{residual crosstalk}} + \underbrace{\sum_{i\in\mathcal{U}} \left|[\mathbf{G}^c]_{ui}\right|^2 \sigma_i^c}_{\text{enhanced noise by ZF}} . \tag{2.6}$$

The ZF-canceler matrix $\mathbf{G}^c$ is given by $\mathbf{G}^c = {\mathbf{H}_{\text{est}}^c}^{-1}$, where $\mathbf{H}_{\text{est}}^c$ denotes the estimate of the channel matrix $\mathbf{H}^c = \mathbf{H}_{\text{est}}^c + \mathbf{E}^c$, and $\mathbf{E}^c$ is the estimation error matrix with element-wise variances $\delta_{ij}^c = \mathsf{E}(|[\mathbf{E}^c]_{ij}|^2)$. δ_{ij}^c, $\forall i,j \in \mathcal{U}\setminus k$, are the channel estimation error variances of the vectoring group lines. δ_{ij}^c with either i or j equal to k are the channel estimation error variances into and from line k, respectively (δ_{kk}^c is the direct channel estimation error variance of line k). The relative channel estimation error ξ_{ij}^c is defined as

$$\xi_{ij}^c = \frac{\delta_{ij}^c}{\left|[\mathbf{H}^c]_{ij}\right|^2}.$$

The noise $\hat{\sigma}_{u,\text{ZF}}^c$ in (2.6) can be divided into noise originating from the vectored lines, $\bar{\sigma}_{u,\text{ZF}}^c$ and noise originating from the joining line k, $\tilde{\sigma}_{u,\text{ZF}}^c$:

$$\hat{\sigma}_{u,\text{ZF}}^c = \bar{\sigma}_{u,\text{ZF}}^c + \tilde{\sigma}_{u,\text{ZF}}^c, \tag{2.7}$$

where

$$\bar{\sigma}_{u,\text{ZF}}^c = \sum_{i,j\in\mathcal{U}\setminus k} \left|[\mathbf{G}^c]_{ui}\right|^2 \delta_{ij}^c p_j^c + \sum_{i\in\mathcal{U}\setminus k} \left|[\mathbf{G}^c]_{ui}\right|^2 \sigma_i^c,$$

[3]Since in practice the FEXT couplings between the lines are different, for each particular tone only one line might experience the predefined maximum increased noise level.

and

$$\tilde{\sigma}^c_{u,\mathrm{ZF}} = \sum_{i\in\mathcal{U}} |[\mathbf{G}^c]_{ui}|^2 \delta^c_{ik} p^c_k + \sum_{j\in\mathcal{U}\setminus k} |[\mathbf{G}^c]_{uk}|^2 \delta^c_{kj} p^c_j + |[\mathbf{G}^c]_{uk}|^2 \sigma^c_k. \tag{2.8}$$

As in Case 1, we limit the maximum noise level using the parameter $q \geq 1$:

$$\hat{\sigma}^c_{u,\mathrm{ZF}} \leq q\bar{\sigma}^c_{u,\mathrm{ZF}}. \tag{2.9}$$

Based on (2.7), (2.8), and (2.9), we are able to calculate the maximum transmit PSD of user k by

$$p^{c,\max}_{k,\mathrm{ZF}} = \min_{u\in\mathcal{U}\setminus k} \frac{\bar{\sigma}^c_{u,\mathrm{ZF}}(q-1) - \sum_{j\in\mathcal{U}\setminus k} |[\mathbf{G}^c]_{uk}|^2 \delta^c_{kj} p^c_j - |[\mathbf{G}^c]_{uk}|^2 \sigma^c_k}{\sum_{i\in\mathcal{U}} |[\mathbf{G}^c]_{ui}|^2 \delta^c_{ik}}. \tag{2.10}$$

The achievable bitrate in bits per multicarrier symbol for user k on tone c in upstream direction is given by

$$r^c_{k,\mathrm{ZF}} = \log_2\left(1 + \frac{\min\left(p^{c,\max}_{k,\mathrm{ZF}}, p^{c,\mathrm{mask}}_k\right)}{\Gamma\hat{\sigma}^c_{k,\mathrm{ZF}}}\right). \tag{2.11}$$

Downstream: With DP and imperfect channel estimation, the noise variance for user u on tone c can be calculated based on [15] yielding

$$\hat{\sigma}^c_{u,\mathrm{DP}} = \sum_{j,i\in\mathcal{U}} \delta^c_{ui} |[\mathbf{G}^c]_{ij} [\mathbf{H}^c_{\mathrm{est}}]_{jj}|^2 p^c_j + \sigma^c_u.$$

Under the assumption that

$$\hat{\sigma}^c_{u,\mathrm{DP}} \leq q\bar{\sigma}^c_{u,\mathrm{DP}},$$

the derivation of the maximum transmit PSD of user k for DP follows, *mutatis mutandis*, the derivation for the ZF and yields

$$p^{c,\max}_{k,\mathrm{DP}} = \min_{u\in\mathcal{U}\setminus k} \frac{\bar{\sigma}^c_{u,\mathrm{DP}}(q-1) - \sum_{j\in\mathcal{U}\setminus k} \delta^c_{ui} |[\mathbf{G}^c]_{ij} [\mathbf{H}^c_{\mathrm{est}}]_{jj}|^2 p^c_j}{\sum_{i\in\mathcal{U}} \delta^c_{ui} |[\mathbf{G}^c]_{ij} [\mathbf{H}^c_{\mathrm{est}}]_{jj}|^2}, \tag{2.12}$$

where

$$\bar{\sigma}^c_{u,\mathrm{DP}} = \sum_{i,j\in\mathcal{U}\setminus k} \delta^c_{ui} \left| \left[\mathbf{G}^c\right]_{ij} \left[\mathbf{H}^c_{\mathrm{est}}\right]_{jj} \right|^2 p^c_j + \sigma^c_u.$$

The achievable bitrate in bits per multicarrier symbol for user k on tone c in downstream direction is given by

$$r^c_{k,\mathrm{DP}} = \log_2 \left(1 + \frac{\left|\left[\mathbf{H}^c_{\mathrm{est}}\right]_{kk}\right|^2 \min\left(p^{c,\max}_{k,\mathrm{DP}}, p^{c,\mathrm{mask}}_k\right)}{\Gamma \hat{\sigma}^c_{k,\mathrm{DF}}} \right). \tag{2.13}$$

2.4 TIME VARIATION OF VECTOR CHANNELS: MEASUREMENT RESULTS

Characterizing the time variation of channel properties observed in a wireline network is a challenge. A slow change of parameters in a vector channel is to be expected due to changes of environmental conditions such as temperature, humidity, or aging of materials. Faster changes may occur due to, for example, changes of termination impedances or a wiggling cable-end caused by a user moving a modem. To the authors' best knowledge, there are no experimental results on the time variation of vector channels available in the open literature. The purpose of this section is to provide some initial evidence on the time variation of vector channels to be expected in real systems.

With a commercial VDSL2 vectoring platform, 6 FEXT coupling functions on 50 tones were recorded roughly every 10 minutes during 8.5 hours yielding 52 data sets. Using the first set as reference, 51 sets of normalized errors were computed. Figure 2.2 shows a histogram and the empirical complementary cumulative distribution function (CCDF) of ξ in % based on the 15300 measurements (the measured errors showed no particular trend over time). 78.2% of the measured errors are below 0.1%, 95.2% are below 0.5%, and 97.6% are below 1%. Note that these results include all the contributing effects to be expected when tracking coefficients with real-world modem equipment (i.e., noise, analog front-end effects, automatic gain scalings, finite precision effects, and coefficient representation).

2.5 SIMULATIONS AND DISCUSSION

This section presents bitrate results of the fast initialization scheme for an example scenario. We consider 15 users in a tree-type network topology with loop lengths between 190 m and 550 m as shown in Figure 2.3. The users are numbered from 1 to 15 and sorted according to line length in increasing order. We use simulation parameters matching the VDSL2 standard

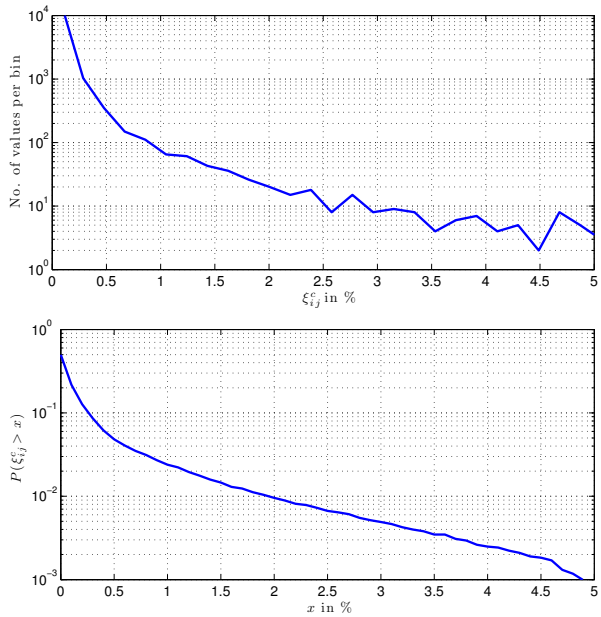

Figure 2.2: Histogram (top) and CCDF (bottom) for measured normalized channel estimation error $\tilde{\xi}_{ij}^c$ in %. Note that the y-axis of the histogram is in logarithmic scale. Bin size 0.1%. 51 consecutive measurements of errors of 6 FEXT coupling functions ($i \in \{1,2,3,4\}$, $j \in \{i+1,\ldots,4\}$) on 50 tones ($c \in \{2792, 2808, \ldots, 3576\}$, tone-group size 16) yield 15300 samples. 24-pair 0.5 mm-cable of 300 m length.

ITU G.993.2 [17] with profile 17a, spectral mask definition EU-32, a maximum transmitted power of 14.5 dBm, a background noise level of -135 dBm/Hz, and maximum bitloading of 15 bits.

The new user is user no. k. Users in $\mathcal{U} \setminus k$ form a vectoring group and we assume that they have perfect knowledge of both direct and FEXT channel coefficients ($\delta_{ij}^c = 0$, $\forall i,j \in \mathcal{U} \setminus k$). The maximum SNR decay of users in the vectoring group caused by user k is $q = 2$ dB, which allows the vectored users to maintain their bitrates.

Case 1: The new user no. k immediately transmits with reduced power but without joining the vectoring group. Figure 2.4 shows the achieved bitrates in downstream and upstream directions for the new user no. k transmitting as "controlled alien". For reference, the bitrates for full vectoring (all 15 users are part of the vectoring group) are shown as well (solid lines). In upstream

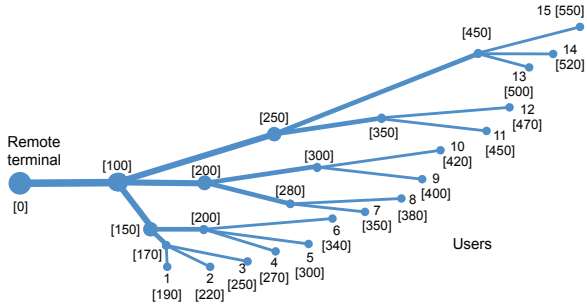

Figure 2.3: Example network topology: 15 users with loop lengths between 190 and 550 m. Users are numbered from 1 to 15 in ascending order according to loop length. Figures in square brackets are distances from the remote terminal in meters.

direction, the bitrate of a new user with a long loop (no. ..., 14, 15) is in the order of 20–55% of the bound achieved with full vectoring. For a user with a short loop (no. 1, 2, ...), however, the upstream bitrate is in the order of 6–15% of the bound since the transmit power has to be reduced drastically in order to protect the weak signals of distant users arriving at the remote terminal. In downstream direction, the bitrates are in the order of 25–37% of the bound.

Case 2: The new user no. k immediately joins the vectoring group after the handshake-phase. While users in the vectoring group have perfect knowledge of both direct and FEXT channel coefficients ($\delta_{ij}^c = 0, \forall i,j \in \mathcal{U} \setminus k$), the new user no. k operates with a channel estimation error ξ ($\xi_{ij}^c \leq \xi, \forall i = k, j \in \mathcal{U} \setminus k, \forall j = k, i \in \mathcal{U} \setminus k$). Figures 2.5 and 2.6 show the achieved bitrates in downstream and upstream direction, respectively. In downstream direction, the achievable bitrate for $\xi \leq 1\%$ is at least 70% of the bound. Even for $\xi = 10\%$, the achievable bitrate is at least 35% of the bound. For large ξ, joining the vectoring group makes no longer sense, since operation as "controlled alien" yields higher bitrates. The ξ level defining the cross-over point between the two cases is in general lower for shorter loops (for example, $\xi \approx 10\%$ for user no. 1).

The performance in upstream direction has essentially the same behavior as in downstream direction. For $\xi = 1\%$, the achievable bitrates drop to around 70% of the bound. For large ξ, operating the user no. k as a "controlled alien" achieves higher bitrates compared to joining the vectoring group. The ξ level defining the cross-over point between the two cases is in general lower for longer loops (cf. loops no. 14 and 15).

It is important to note that only a few users experience a noise-margin decay

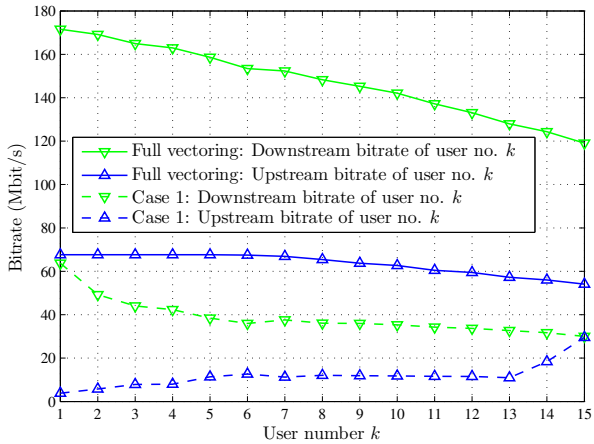

Figure 2.4: Bitrates for Case 1 ($q = 2\,\text{dB}$).

as large as the limit of $q = 2\,\text{dB}$. The actual noise-margin decay depends on the transmit PSD and the FEXT coupling functions, which depend on both frequency and coupling length. Figure 2.7 shows the noise-margin decay in downstream direction for users no. 1, 2, ..., 6, 7, 9, 10, ..., 15 caused by user no. 8 joining the vectoring group with $\xi = 5\,\%$. For tones up to index 523, only user no. 7 experiences the full noise-margin decay of 2 dB. Due to the mid-range coupling length of 280 m (FEXT post-attenuation 70 m), line no. 7 sees the strongest FEXT coupling from line no. 8 for low frequencies (cf. Figure 2.8). For tones above index 523, only line no. 1 experiences the full 2 dB of noise-margin decay since the FEXT coupling from line no. 8 into line no. 1 dominates (coupling length 100 m, FEXT post-attenuation 90 m).

Figure 2.9 shows the downstream bitrate of user no. 8 for different q and ξ values. A higher noise limit q yields a higher bitrate. An increase in q from 0.5 dB to 3 dB results in a bitrate increase of approximately 16%, 45%, and 16% (or equivalently, 12%, 13%, and 3% of the full-vectoring bound) for ξ equal to 0.5%, 10%, and 50%, respectively.

2.6 CONCLUSION

Vectoring is a pre-requisite for exploiting the capacity of wireline networks. Initialization of vectored systems is crucial. Procedures currently proposed in standards require a considerable amount of time for initialization before a new user can transmit or receive payload data. In this paper, a fast initialization for vectored systems based on spectral protection is analyzed,

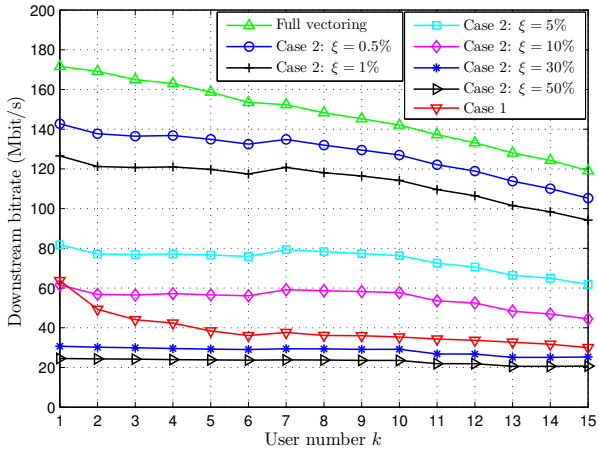

Figure 2.5: Downstream bitrates for Case 2 ($q = 2\,\text{dB}$).

that allows users to transmit and receive immediately after the handshake phase without threatening system stability. The scheme can be merged with existing standards (most importantly, VDSL2) and yields an improved user experience through immediate connectivity after start-up. The achievable bitrates depend strongly on the available channel knowledge. For channel errors in the order of 1%, bitrates around 70% of the full-vectoring bound can be achieved.

ACKNOWLEDGMENT

This work was partly supported by the Swedish Research Council (VR) through grant No. 621-2007-6309 and by the Swedish Foundation for Strategic Research (SSF) through grant No. ICA08-0022. The Competence Center FTW Forschungszentrum Telekommunikation Wien GmbH is funded within the program COMET - Competence Centers for Excellent Technologies by BMVIT, BMWFJ, and the City of Vienna. The COMET program is managed by the FFG.

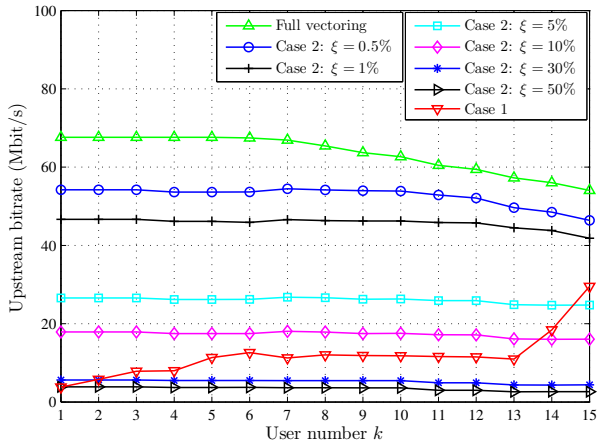

Figure 2.6: Upstream bitrates for Case 2 ($q = 2\,\mathrm{dB}$).

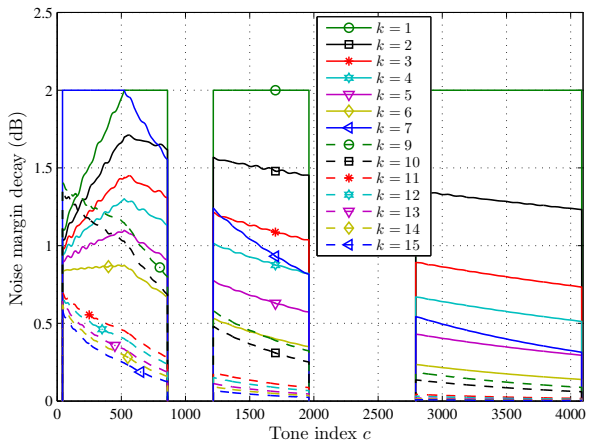

Figure 2.7: Downstream noise-margin decay caused by user no. 8 ($k = 8$) for Case 2 ($q = 2\,\mathrm{dB}$, $\xi = 5\,\%$).

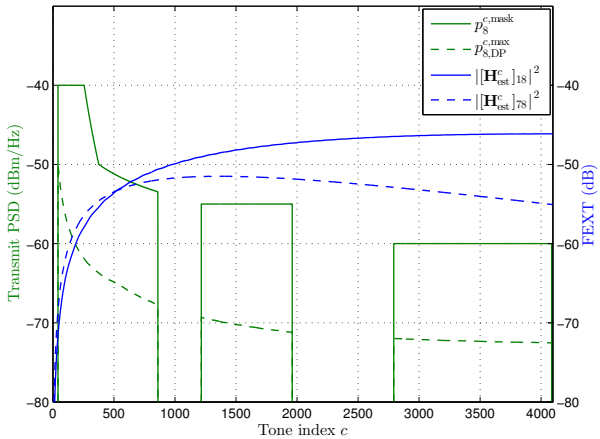

Figure 2.8: Left axis: transmit PSD mask and transmit PSD of user no. 8. Right axis: squared FEXT coupling magnitude from user no. 8 to users no. 1 and no. 7 ($q = 2\,\mathrm{dB}$, $\xi = 5\,\%$).

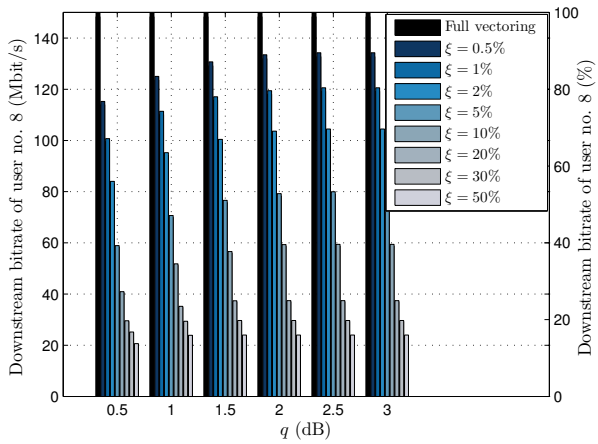

Figure 2.9: Downstream bitrate of user no. 8 for different q and ξ values.

References

[1] K. B. Song, S. T. Chung, G. Ginis, and J. M. Cioffi, "Dynamic spectrum management for next-generation DSL systems," *IEEE Communications Magazine*, vol. 40, no. 10, pp. 101–109, Oct. 2002.

[2] G. Ginis and J. M. Cioffi, "Vectored transmission for digital subscriber line systems," *IEEE Journal on Selected Areas in Communications*, vol. 20, no. 5, pp. 1085–1104, Jun. 2002.

[3] R. Cendrillon, M. Moonen, J. Verlinden, T. Bostoen, and G. Ginis, "Improved linear crosstalk precompensation for DSL," in *Proc. IEEE International Conference on Acoustics, Speech, and Signal Processing (ICASSP), 2004*, vol. 4, Montreal, Quebec, Canada, May 2004, pp. 1053–1056.

[4] R. Cendrillon, M. Moonen, E. Van den Bogaert, and G. Ginis, "The linear zero-forcing crosstalk canceler is near-optimal in DSL channels," in *Proc. IEEE Global Telecommunications Conference (GLOBECOM 2004)*, vol. 4, Dallas, TX, USA, Nov.–Dec. 2004, pp. 2334–2338.

[5] R. Cendrillon, M. Moonen, G. Ginis, K. Van Acker, T. Bostoen, and P. Vandaele, "Partial crosstalk cancellation for upstream VDSL," *EURASIP J. Appl. Signal Process.*, vol. 2004, no. 10, pp. 1520–1535, Jan. 2004. [Online]. Available: http://dx.doi.org/10.1155/S1110865704309273

[6] R. Cendrillon, G. Ginis, M. Moonen, and K. Van Acker, "Partial crosstalk precompensation in downstream VDSL," *Signal Process.*, vol. 84, no. 11, pp. 2005–2019, Nov. 2004. [Online]. Available: http://dx.doi.org/10.1016/j.sigpro.2004.07.013

[7] R. Cendrillon, G. Ginis, E. Van den Bogaert, and M. Moonen, "A Near-Optimal Linear Crosstalk Canceler for Upstream VDSL," *IEEE Transactions on Signal Processing*, vol. 54, no. 8, pp. 3136–3146, Aug. 2006.

[8] ——, "A Near-Optimal Linear Crosstalk Precoder for Downstream VDSL," *IEEE Transactions on Communications,*, vol. 55, no. 5, pp. 860–863, May 2007.

[9] ITU, *Very high speed digital subscriber line transceivers 2 (VDSL2), Technical Recommendation G.993.2*, ITU Std., Dec. 2011.

[10] V. Oksman, H. Schenk, A. Clausen, J. M. Cioffi, M. Mohseni, G. Ginis, C. Nuzman, J. Maes, M. Peeters, K. Fisher, and P.-E. Eriksson, "The ITU-T's new G.vector standard proliferates 100 Mb/s DSL," *IEEE Communications Magazine*, vol. 48, no. 10, pp. 140–148, Oct. 2010.

[11] ITU, *Self-FEXT Cancellation (Vectoring) for Use with VDSL2 Transceivers, Technical Recommendation G.993.5*, ITU Std., Apr. 2010.

[12] Alcatel, "G.vdsl: MIMO for VDSL2: Requirements to allow upstream MIMO," Contribution TD HH-56 to ITU Study Group 15, ITU, Jan. 2005.

[13] ——, "G.vdsl: MIMO for VDSL2: Requirements to allow downstream MIMO," Contribution TD HH-57 to ITU Study Group 15, ITU, Jan. 2005.

[14] P. Whiting, A. Ashikhmin, G. Kramer, C. Nuzman, A. Van Wijngaarden, M. Zivkovic, M. Peeters, M. Guenach, J. Maes, and J. Verlinden, "DSL Crosstalk Coefficient Acquisition Using SNR Feedback," in *Proc. IEEE Global Telecommunications Conference (GLOBECOM 2008)*, New Orleans, LA, USA, Nov.–Dec. 2008, pp. 1–5.

[15] G. Marrocco, M. Wolkerstorfer, T. Nordström, and D. Statovci, "Energy-Efficient DSL using Vectoring," in *Proc. IEEE Global Telecommunications Conference (GLOBECOM 2011)*, Houston, TX, USA, Dec. 2011, pp. 1–6.

[16] J. Huang, V. Subramanian, R. Agrawal, and R. Berry, "Downlink scheduling and resource allocation for OFDM systems," *IEEE Transactions on Wireless Communications*, vol. 8, no. 1, pp. 288–296, Jan. 2009.

[17] ITU, *Very high speed digital subscriber line transceivers 2 (VDSL2), Technical Recommendation G.993.2*, ITU Std., July 2002.

3

How Vectoring in G.fast May Cause Neighborhood Wars

Eduardo Medeiros, Thomas Magesacher, Per-Erik Eriksson, Chenguang Lu and Per Ödling

Abstract

Emerging wireline transmission systems such as G.fast use bands up to around 200 MHz on short cables. A key enabler for achieving the aspired throughput of several hundred Mbit/s is joint processing of transmit signals in downstream direction as well as joint processing of receive signals in upstream direction through techniques referred to as vectoring. A new challenge in such systems are sudden and severe changes in the channel matrix caused by changing terminations on lines *outside* the vectoring group. Such events can be caused by users disconnecting their modems, turning them on or off, or on-/off-hook events on lines that still support the plain old telephony service.

This work presents channel measurements capturing the impact of termination changes caused by modems or handsets. An analysis of the impact of these sudden changes on the signal-to-noise-power-ratio in vectoring systems reveals that throughput and stability can be seriously degraded. The potential of decision-directed channel tracking based on least squares estimation is investigated.[1]

[1]Published in *Proc. IEEE International Conference on Communications (ICC 2014)*, Sydney, NSW, 10-14 Jun. 2014.

3.1 INTRODUCTION

The implementation of precoding and crosstalk cancellation schemes has enabled multi-carrier copper-based systems to reach bit rates around 100 Mbit/s [1] [2]. These advances have prolonged the life expectancy of copper cables in the field, while allowing operators to extend their fiber-based access network to distribution points, avoiding the massive investment step of deploying fiber to the customer premises.

As deployments of vectored VDSL2 hit the market, vendors and academia [3] have been involved in drafting a new standard (G.fast), with features that support even higher bit-rates, improved energy efficiency through discontinuous operation and enable new business models through reverse powering.

One of the practical challenges of deploying vectored VDSL2 schemes is referred to in the literature as disorderly leaving events (DLEs). A DLE happens when one of the lines in the vectoring group is disconnected or powered off. This causes the termination impedance to change and consequently a change in the crosstalk coupling gains. When dealing with DLEs, the ITU-G.vector standard [1] advises implementors to mute (turn off) transmitters as soon as possible. DLEs have been addressed in [4] by means of a fast tracking algorithm. That work has influenced a corrigendum to the standard [5], where a procedure for fast precoder coefficient update is described.

Differently from its predecessors, G.fast will be a time-division duplex (TDD) system. One of the envisioned features, the so-called discontinuous operation, allows transceivers to switch to an energy-saving mode during portions of a TDD frame where there is no useful data to send. This has serious implications for the vectoring engine design [6]. In a precoding scheme, for example, turning off some transceivers is equivalent to changing the size of the precoding matrix—a change that requires precoder coefficient recalculation and transmit power spectral density (PSD) adjustment [7]. Several contributions have been presented to address this issue [8] [9].

One point that these contributions stress is the assumption that discontinuous operation does not change the impedance of the line. If impedances were to change, the far-end crosstalk (FEXT) couplings would be modified in the whole channel matrix, requiring a lengthy channel estimation phase prior to the precoder update.

In a recent ITU contribution [10], it is suggested that G.fast vectoring bundles may be affected by changes in the terminating impedance of alien lines, that is, lines which are *not part* of the vectoring group. While a DLE occurs with lines which are part of a vectoring group, and are therefore monitored and managed as a unit, in G.fast this change can be triggered by any neighboring line, such as a plain old telephony service (POTS) line in the same cable or even by a line managed by a different operator.

This paper focuses on the impact of alien-line termination changes caused by modems or POTS handsets and investigates possible remedies. In Section 3.2, the system model and an analysis of the signal-to-noise-power-ratio (SNR) are introduced. Section 3.3 presents measurement and SNR-loss results. Section 3.4 investigates the potential of decision-directed channel tracking based on least-squares estimation and Section 3.5 concludes the work.

3.2 SYSTEM MODEL AND ANALYSIS

Hereinafter, the following notation is used: bold upper-case and bold lower-case symbols are used to denote matrices and vectors, respectively. $\boldsymbol{X}(i,j)$ denotes the element in row i and column j of $\boldsymbol{X}$ and $\otimes$ is the Kronecker product.

3.2.1 VECTORED TRANSMISSION

For a discrete multi-tone (DMT) system using TDD with U synchronised transmitters and a cyclic prefix of sufficient length, the received symbol vector $\boldsymbol{y}_k^\ell \in \mathbb{C}^{U\times 1}$ at time instant k for subcarrier no. ℓ can be modelled in frequency-domain as

$$\boldsymbol{y}_k^\ell = \boldsymbol{H}_k^\ell \boldsymbol{x}_k^\ell + \boldsymbol{n}_k^\ell, \tag{3.1}$$

where $\boldsymbol{x} \in \mathbb{C}^{U\times 1}$ is the transmitted symbol vector, $\boldsymbol{H} \in \mathbb{C}^{U\times U}$ is the frequency-domain channel matrix and $\boldsymbol{n} \in \mathbb{C}^{U\times 1}$ is the additive noise vector. For the sake of simplicity, time index k and subcarrier index ℓ are omitted when possible.

Since near-end crosstalk (NEXT) can be disregarded, the received symbol for user $u \in \{1,\ldots,U\}$ can be written as

$$\boldsymbol{y}(u) = \boldsymbol{H}(u,u)\boldsymbol{x}(u) + \sum_{m\neq u} \boldsymbol{H}(u,m)\boldsymbol{x}(m) + \boldsymbol{n}(u),$$

where the term $\sum_{m\neq u} \boldsymbol{H}(u,m)\boldsymbol{x}(m)$ represents FEXT.

Given that the channel matrix $\boldsymbol{H}$ is known, FEXT can be mitigated by means of low-complexity linear compensation schemes. The zero-forcing canceler [11] and the diagonalizing precoder [12] provide near optimal performance for upstream and downstream directions, respectively.

This paper deals with imperfect channel information caused by changes in an *alien line's* terminating impedance. Alien lines are defined as copper pairs which are not part of the vectoring group but might, for example, share portions of the the same cable or even the same binder.

It is reasonable to assume that all lines at the distribution point are properly terminated. On the customer premises side, however, the alien line's terminating impedance could change, as a result of equipment being powered off,

disconnected or even, in case of a POTS handset, being taken on/off hook. In order to model this situation, we use the channel model (3.1) with two distinct states $\boldsymbol{H} = \boldsymbol{T}$ and $\boldsymbol{H} = \boldsymbol{O}$, where the channel matrix $\boldsymbol{T}$ represents the state when the alien line is properly terminated (i.e. a 100 Ω resistor or an on-hook phone is connected) and $\boldsymbol{O}$ represents the state when the alien line is left open (or an off-hook phone is connected). $\boldsymbol{T}$ and $\boldsymbol{O}$ can be related by

$$\boldsymbol{O} = \boldsymbol{T} + \boldsymbol{\Delta}, \tag{3.2}$$

where the matrix $\boldsymbol{\Delta}$ represents the mismatch in complex channel coefficients due to the terminating impedance change.

The next sections present expressions for the SNR in upstream and downstream using the aforementioned zero-forcing canceler and diagonalizing precoder, respectively. For a full derivation of these expressions, see [13]. We distinguish between the SNR before the termination change, denoted $SNR^{\boldsymbol{T}}$, and the SNR after the termination change, denoted $SNR^{\boldsymbol{O}}$, and define the SNR loss ΔSNR_u for user u in dB as

$$\Delta SNR_u = 10 \log_{10} SNR_u^T - 10 \log_{10} SNR_u^O. \tag{3.3}$$

3.2.2 UPSTREAM: PERFORMANCE OF ZERO-FORCING WITH IMPERFECT CHANNEL ESTIMATES

In upstream direction, the received symbol $\boldsymbol{z}(u)$ for user u is given by

$$\boldsymbol{z}(u) = \boldsymbol{x}(u) + \sum_{i \in \mathcal{U}} \sum_{j \in \mathcal{U}} \boldsymbol{T}^{-1}(u,i) \boldsymbol{\Delta}(i,j) \boldsymbol{x}(j) + \sum_{i \in \mathcal{U}} \boldsymbol{T}^{-1}(u,i) \boldsymbol{n}(i),$$

where $\mathcal{U} \subset \{1, \ldots, U\}$ is the set of active transmitters. The term $\sum_{i \in \mathcal{U}} \sum_{j \in \mathcal{U}} \boldsymbol{T}^{-1}(u,i) \boldsymbol{\Delta}(i,j) \boldsymbol{x}(j)$ is the residual crosstalk caused by the alien line's termination change. Here, we assume that the estimate of the channel before a termination change, $\boldsymbol{T}$, is perfect.

The SNR for user u before the termination change can be written as

$$SNR_u^T = \frac{p_u}{\Gamma \left(\sum_{i \in \mathcal{U}} |\boldsymbol{T}^{-1}(u,i)|^2 \sigma_i \right)}, \tag{3.4}$$

where Γ is the SNR-gap to capacity, $p_i = \mathsf{E}\left\{ |\boldsymbol{x}(i)|^2 \right\}$ is the variance of the transmitted symbol at user i and $\sigma_i = \mathsf{E}\left\{ |\boldsymbol{n}(i)|^2 \right\}$ is the variance of the additive noise experienced by user $i \in \mathcal{U}$.

After the alien line termination is removed, the SNR for user u can be calculated as

$$SNR_u^O = \frac{p_u}{\Gamma\left(\sum_{i\in\mathcal{U}}\sum_{j\in\mathcal{U}}|\boldsymbol{T}^{-1}(u,i)|^2\boldsymbol{\Phi}(i,j)p_j + \sum_{i\in\mathcal{U}}|\boldsymbol{T}^{-1}(u,i)|^2\sigma_i\right)}, \tag{3.5}$$

where $\boldsymbol{\Phi}(i,j) = \mathsf{E}\left\{|\boldsymbol{\Delta}(i,j)|^2\right\}$ is the channel estimation error variance.

3.2.3 DOWNSTREAM: PERFORMANCE OF DIAGONALIZING PRECODER WITH IMPERFECT CHANNEL ESTIMATES

In downstream direction, the received symbol $\boldsymbol{z}'(u)$ at user u can be written as

$$\boldsymbol{z}'(u) = \boldsymbol{D}(u,u)\boldsymbol{x}(u) + \sum_{i\in\mathcal{U}}\sum_{j\in\mathcal{U}}\boldsymbol{\Delta}(u,i)\boldsymbol{T}^{-1}(i,j)\boldsymbol{D}(j,j)\boldsymbol{x}(j) + \boldsymbol{n}(u),$$

where $\boldsymbol{D}$ is a diagonal matrix with $\boldsymbol{D}(u,u) = \boldsymbol{T}(u,u)$.

Before the termination change, the SNR for user u is given by

$$SNR_u^T = \frac{|\boldsymbol{T}(u,u)|^2 p_u}{\Gamma\,\sigma_u}. \tag{3.6}$$

After the termination change, the SNR for user u can then be calculated as

$$SNR_u^O = \frac{|\boldsymbol{T}(u,u)|^2 p_u}{\Gamma\left(\sum_{i\in\mathcal{U}}\sum_{j\in\mathcal{U}}\boldsymbol{\Phi}(u,i)\left|\boldsymbol{T}^{-1}(i,j)\boldsymbol{T}(j,j)\right|^2 p_j + \sigma_u\right)}, \tag{3.7}$$

assuming perfect knowledge of the channel before the termination change.

3.3 EXPERIMENTAL RESULTS

This section presents experimental evidence that corroborates the significant impact of alien lines' termination changes on vectored G.fast performance. Measured channel information is used to compare the performance of linear compensation schemes before and after a termination change.

3.3.1 MEASUREMENT SETUP

The experimental setup is depicted in Fig. 3.1 and consists of a 30-pair cable (0.5 mm, 100 m) with three binders. Six lines of the same binder are chosen

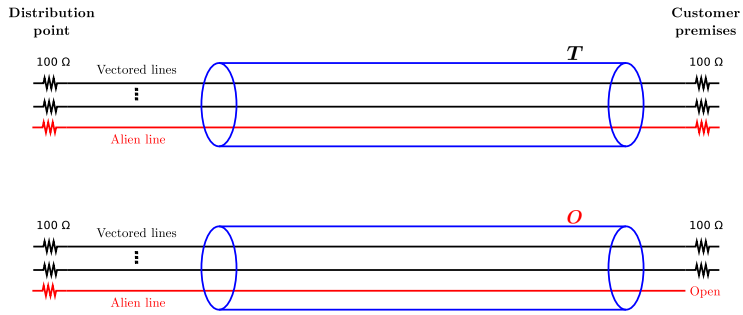

Figure 3.1: Experimental setup. When all lines are properly terminated, the matrix $\boldsymbol{T}$ is measured (top). After the alien line termination is removed, $\boldsymbol{O}$ is measured (bottom).

to constitute a 5-line vector group and an alien line. The measurement equipment (a network analyzer) is coupled to the vectored copper pairs using 100 Ω balun transformers. The alien line extremity at the distribution point is at all times terminated in a 100 Ω resistor.

The other end of the alien line is initially coupled to a 100 Ω resistor. This load represents the purely resistive impedance of a G.fast modem [14]. A first set of transfer function measurements is taken, constituting the $\boldsymbol{T}$ matrix. Next, the resistor is removed and a new batch of measurements are performed and stored in matrix $\boldsymbol{O}$. This procedure was executed for both downstream and upstream directions.

The stability and accuracy of the measurement setup has been verified following the procedures described in [10]. The measurements were performed under the following assumptions:

- 51.75 KHz subcarrier spacing.
- The first 3500 subcarriers are considered.
- No interpolation has been used (exactly one measurement point per subcarrier).

A sample of the measurement results is shown in Fig. 3.2. The upper subplot presents the squared magnitude of $\boldsymbol{T}(4,1)$ and $\boldsymbol{O}(4,1)$ for the downstream direction. The lower subplot presents the squared magnitude of the ratio between $\boldsymbol{O}(4,1)$ and $\boldsymbol{T}(4,1)$ in dB.

3.3.2 VECTORING PERFORMANCE COMPARISON

The measured channel matrix $\boldsymbol{T}$ has been used to train a diagonalizing precoder and zero-forcing canceler. Fig. 3.3 presents the resulting SNRs for line 4

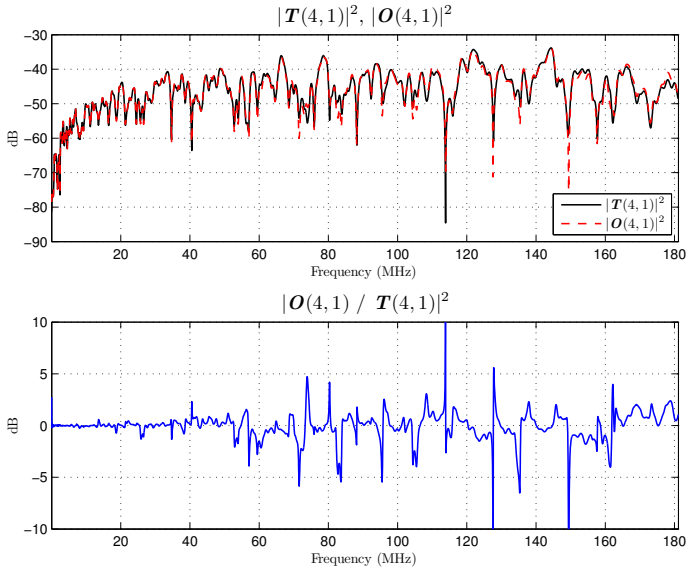

Figure 3.2: Top: Squared magnitude of FEXT coupling coefficients from line 1 into line 4 before ($\boldsymbol{T}$) and after ($\boldsymbol{O}$) the alien-line termination change. Bottom: Impact of termination change in terms of the ratio between $\boldsymbol{O}$ and $\boldsymbol{T}$ in dB.

(worst case). The black lines in Fig. 3.3 correspond to the crosstalk-free SNRs achieved with perfect channel knowledge ($SNR^{\boldsymbol{T}}$) when using diagonalizing precoding in downstream (top plot) and zero forcing in upstream (bottom plot). The SNR calculations presented in this section assume a transmit PSD of $-76\,\mathrm{dBm/Hz}$, a background-noise PSD of $-140\,\mathrm{dBm/Hz}$, and $\Gamma = 12.9\,\mathrm{dB}$.

The red solid lines represent the SNRs achieved after the alien line termination changes ($SNR^{\boldsymbol{O}}$). The precoder/canceler settings are outdated and the residual crosstalk terms in $\boldsymbol{\Delta}$ cause a considerable performance degradation (see (3.5) and (3.7)).

The areas filled in blue in Fig. 3.3 represent the total SNR loss (ΔSNR) caused by the alien line termination change. For both directions, more than half of the subcarriers experience a SNR degradation larger than 6 dB.

Fig. 3.4 shows the SNR loss ΔSNR for all lines. From these plots it becomes even clearer that the SNR loss caused by the impedance change is significant. Whenever the termination in the alien line changes, all lines in the vector group experience an instantaneous loss in SNR, higher than 6 dB for subcarriers above 60 MHz. For the two worst lines (2 and 4), ΔSNR peaks at around 20 dB.

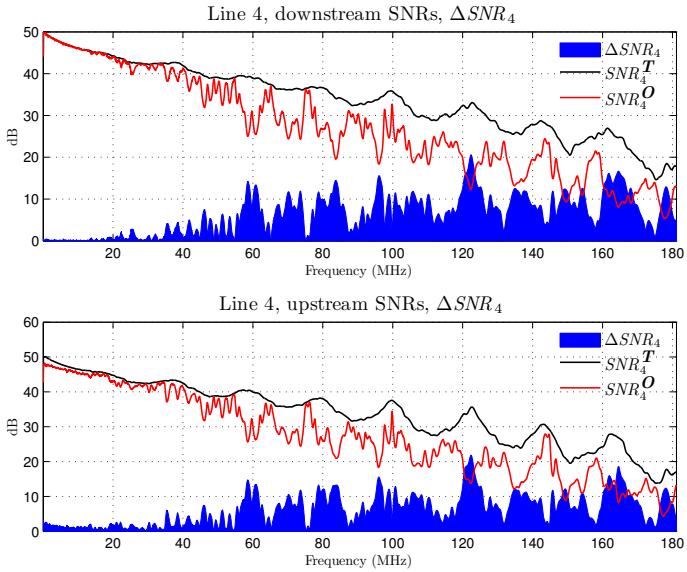

Figure 3.3: SNR comparison for line 4 before and after the alien-line termination change using diagonalizing precoding in downstream direction (top) and zero forcing in upstream direction (bottom). The black line represents SNR_4^T, the SNR before alien line termination change. The red lines represents SNR_4^O, the SNR after the terminating resistor is removed. The area shaded in blue represents ΔSNR_4.

Also in Fig. 3.4, one can notice that the performance of most lines is practically unchanged up to 20 MHz. This fact is worthy of notice because it represents exactly the frequency range used for most of the deployed VDSL2 systems (using 17 MHz profiles). In other words, while this issue is of high impact for G.fast systems, it may have been undetected for VDSL2, which was standardised without requiring channel tracking features.

Fig. 3.5 shows the empirical complementary cumulative distribution function of the ΔSNR based on one set of measurements over the 3500 subcarriers. The curves are very similar for both directions. Three of the five lines in the vector group have between 10 and 15% of their active subcarriers subject to a SNR loss higher than 6 dB. For the worst performing lines, (2 and 4) roughly half of the subcarriers have a ΔSNR higher than 6 dB.

The results shown in Fig. 3.5 hint that state-of-the-art mechanisms used in VDSL2 such as bit-swapping and seamless rate adaptation may not be able to adequately remedy the termination-change problem in G.fast. To illustrate this issue, it is worth picturing a 24-user vectoring group. With just one alien

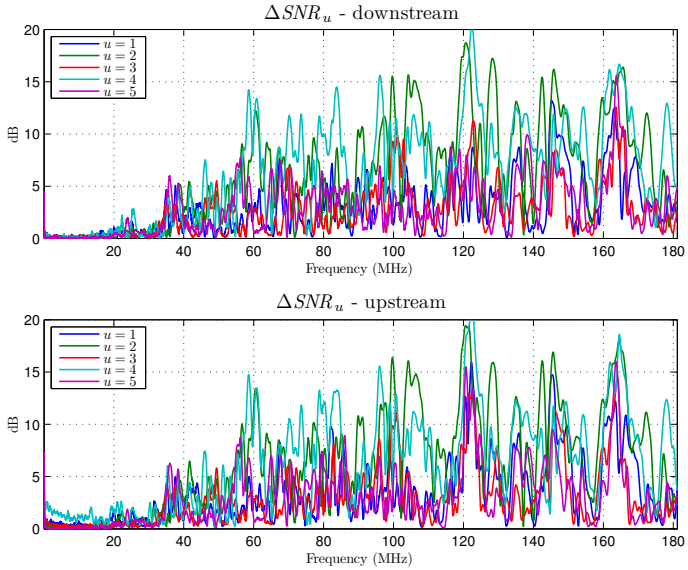

Figure 3.4: SNR loss ΔSNR_u for $u \in \{1, \ldots, 5\}$ when using diagonalizing precoding in downstream direction (top) and zero forcing in upstream direction (bottom).

line impedance change (let's say, an on-off hook transition in a neighboring line) the whole channel matrix would change. Suddenly the whole 24 lines would face a significant SNR loss over hundreds of subcarriers.

3.3.3 IMPACT OF TERMINATION CHANGE IN DIFFERENT VECTOR GROUP SIZES

The SNR loss caused by changes of terminating impedances is more harmful to larger vector groups. Since the whole channel matrix changes, larger vectoring bundles tend to suffer with the error propagation. The experimental data collected by the authors can be used to illustrate the practical effects of this fact.

Fig. 3.6 depicts the SNR loss experienced by line 4 while being part of vectoring groups with different sizes. The vectoring bundles in question use the linear precoder. The SNR loss consistently increases for larger groups, with $U = 5$ being the worst case. For some subcarriers the difference between a $U = 2$ and a $U = 5$ vector group is higher than 6 dB. This SNR loss is higher than the usual 6 dB of target margin used by DSL operators to maintain stability.

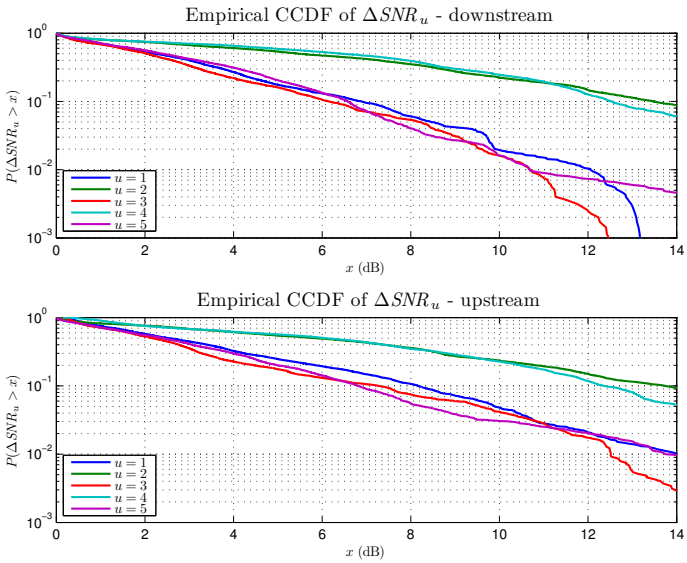

Figure 3.5: Empirical CCDF of the ΔSNR_u defined in (3.3) when using diagonalizing precoding in downstream direction (top) and zero forcing in upstream direction (bottom).

3.4 CHANNEL TRACKING

In this section, we investigate the suitability of decision-directed (blind) channel tracking based on least-squares estimation as a remedy to mitigate the impact of sudden channel changes. The purpose is to verify the concept and point out some basic tradeoffs under typical operating conditions encountered by G.fast systems. Note that a solution for use in practical systems requires optimization of tracking accuracy, stability and complexity for the operating point (SNR margin) at hand.

3.4.1 SLIDING-WINDOW LEAST SQUARES

Hereinafter, we focus on decision-directed channel tracking in upstream direction for a single subchannel of a vectoring system using zero-forcing. In a real system, the tracking has to be extended to all subchannels that experience severe degradation.

Let z_k and $\hat{x}_k$ denote zero-forcing equalizer output and hard decisions for receive symbol no. k, respectively. We use the error $e_k = z_k - \hat{x}_k$ as a measure for the channel deviation Δ caused by a termination change[2]. Under the

[2]In principle, it would of course be desirable to use decisions from the channel

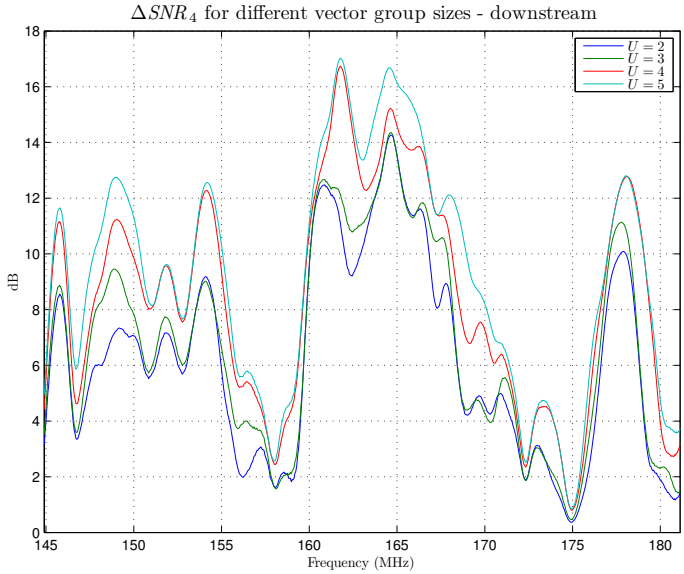

Figure 3.6: ΔSNR_4 for different vectoring group sizes in downstream direction. Residual crosstalk increases with the number of lines.

assumption that the decisions are correct ($\hat{\boldsymbol{x}}_k = \boldsymbol{x}_k$), the error is given by $\boldsymbol{e}_k = \boldsymbol{\Delta}' \hat{\boldsymbol{x}}_k + \boldsymbol{T}^{-1}\boldsymbol{n}_k$, where $\boldsymbol{\Delta}' = \boldsymbol{T}^{-1}\boldsymbol{\Delta}$, and we attempt to "average out" the channel noise $\boldsymbol{T}^{-1}\boldsymbol{n}_k$ by applying the least squares approach.

Let $\boldsymbol{e}_{k,W_k} = \begin{bmatrix} \boldsymbol{e}_k^{\mathrm{T}} & \boldsymbol{e}_{k-1}^{\mathrm{T}} & \dots & \boldsymbol{e}_{k-W_k+1}^{\mathrm{T}} \end{bmatrix}^{\mathrm{T}} \in \mathbb{C}^{UW_k \times 1}$ denote the errors of the last W_k DMT symbols, where W_k is the length of our sliding observation window. Stacking the rows of $\boldsymbol{\Delta}'$ into a vector $\boldsymbol{\delta}' \in \mathbb{C}^{U^2 \times 1}$ and defining the matrix

$$\hat{\boldsymbol{X}}_k = \begin{bmatrix} \boldsymbol{I}_U \otimes \hat{\boldsymbol{x}}_k^{\mathrm{T}} \\ \boldsymbol{I}_U \otimes \hat{\boldsymbol{x}}_{k-1}^{\mathrm{T}} \\ \vdots \\ \boldsymbol{I}_U \otimes \hat{\boldsymbol{x}}_{k-W_k+1}^{\mathrm{T}} \end{bmatrix} \in \mathbb{C}^{W_k U \times U^2},$$

we can write the error vector of the last W_k DMT symbols as $\boldsymbol{e}_{k,W_k} = \hat{\boldsymbol{X}}_k \boldsymbol{\delta}' + \boldsymbol{n}_{k,W_k}$ where $\boldsymbol{n}_{k,W_k} = \left(\boldsymbol{I}_{W_k} \otimes \boldsymbol{T}^{-1}\right) \begin{bmatrix} \boldsymbol{n}_k^{\mathrm{T}} & \boldsymbol{n}_{k-1}^{\mathrm{T}} & \dots & \boldsymbol{n}_{k-W_k+1}^{\mathrm{T}} \end{bmatrix}^{\mathrm{T}}$ denotes the re-

decoder output. However, channel decoder output symbols are only available after a certain delay, which depends on the scheme and the strength of the code at hand. For simplicity, we here focus on uncoded hard decisions.

ceived noise. The least-squares approximation $\hat{\boldsymbol{\delta}}'_k$ of $\boldsymbol{\delta}'_k$ can, for example, be obtained using the pseudoinverse of $\hat{\boldsymbol{X}}_k$ yielding

$$\hat{\boldsymbol{\delta}}'_k = \left(\hat{\boldsymbol{X}}_k^{\mathrm{H}} \hat{\boldsymbol{X}}_k\right)^{-1} \hat{\boldsymbol{X}}_k^{\mathrm{H}} \boldsymbol{e}_{k,W_k}. \tag{3.8}$$

Row-wise stacking of $\hat{\boldsymbol{\delta}}'_k$ into a matrix $\hat{\boldsymbol{\Delta}}'_k$ finally allows us to compute the channel-deviation estimate

$$\hat{\boldsymbol{\Delta}}_k = \boldsymbol{T}\hat{\boldsymbol{\Delta}}'_k.$$

In a real system implementation, the channel tracker can be activated based on an error metric derived from receiver-side hard decisions or based on a metric from a monitoring system detecting a performance decay on all lines in the vectoring group. Clearly, the challenge with blind channel tracking is that the assumption of making correct decisions after the channel change ($\hat{\boldsymbol{x}}_k = \boldsymbol{x}_k$) may not hold. Simulations presented in the following section investigate the impact of decision errors.

3.4.2 CASE STUDY

We use the cable measurements presented in the previous section in a vectoring system with $U = 5$ users and choose the following parameters conforming with the emerging G.fast standard: transmit PSD $-76\,\mathrm{dBm/Hz}$, background noise $-140\,\mathrm{dBm/Hz}$. The channel attenuation at the chosen frequency (subchannel no. $\ell = 3178$, which corresponds to subcarrier frequency 164.4 MHz) is roughly 27 dB yielding a receive SNR of about 37 dB. In order to achieve an uncoded symbol error rate of 10^{-7}, a receive SNR of roughly 28 dB is required for 64-QAM yielding an SNR margin of 9 dB. For 128-QAM, the required receive SNR is roughly 31 dB resulting in an SNR margin of 6 dB. Finally, for 256-QAM, the required SNR is roughly 34 dB with an SNR margin of 3 dB.

We simulate 1000 runs of transmission and channel tracking for 64-QAM, 128-QAM, and 256-QAM where a line outside the vectoring group changes termination right before symbol no. $k = 1$:

$$\boldsymbol{H}_k = \begin{cases} \boldsymbol{T}, & k < 1 \\ \boldsymbol{O} = \boldsymbol{T} + \boldsymbol{\Delta}, & k \geq 1 \end{cases}.$$

Fig. 3.7 shows that the sudden channel change causes an SNR loss of around 16 dB for user $u = 4$.

We invoke the channel tracker (3.8) after every received DMT symbol for $k \geq 1$ in order to show the achievable SNR improvement. In a real system, more complexity-friendly implementations of (3.8) should be employed. From symbol no. $k = 21$ on, the window size is increased linearly from 20 to 80 and

then kept constant:

$$W_k = \begin{cases} 20, & 1 \leq k \leq 20 \\ k, & 21 \leq k \leq 80 \\ 80, & k > 81 \end{cases}.$$

Since wrong decisions during the tracking procedure cause an error bias, there is no notable improvement for $k > 80$. Thus, the tracking can be stopped and the coefficients can be frozen for $W_k > 80$. Note that this choice for the window length is not optimized in any sense. Further work is required to, for example, adjust the window length depending on the residual error in combination with a recursive implementation of the least squares estimator in order to circumvent expensive matrix inversions.

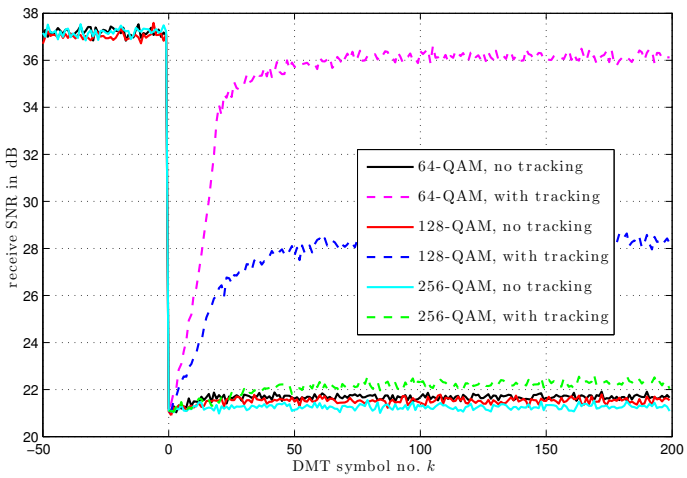

Figure 3.7: Receive SNR of user $u = 4$ with and without tracking for 64-QAM, 128-QAM, and 256-QAM. For $k \geq 1$, a termination change from 100 Ohm to open on the alien line causes a sudden change in the channel matrix. The SNR results shown are averaged over 1000 simulation runs.

Fig. 3.8 shows the cumulative QAM-symbol error count of user $u = 4$ averaged over 1000 simulation runs. For 64-QAM, 128-QAM, and 256-QAM, the symbol error count without tracking continues to rise after the channel change (note the logarithmic scale on the y-axis). Channel tracking essentially avoids errors for 64-QAM apart from a total of 17 QAM-symbol errors in 1000 simulation runs (or equivalently, an average of 0.017 QAM symbol errors) during the tracking phase.

Tracking for 128-QAM manages to reduce the SNR loss from about 15 dB to

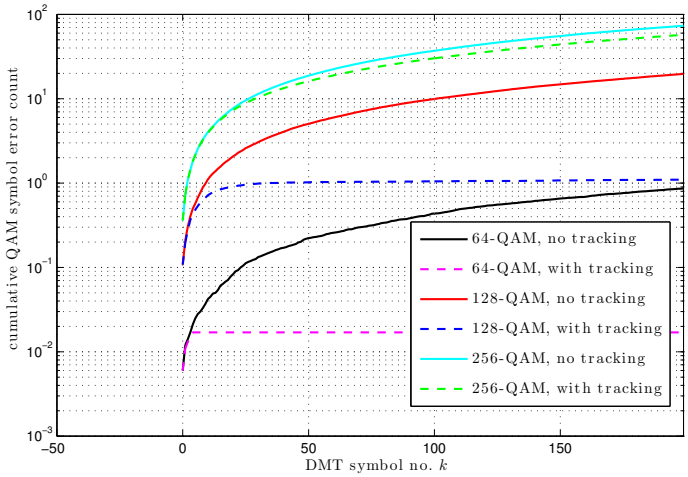

Figure 3.8: Cumulative QAM symbol error count of user $u = 4$ with and without tracking for 64-QAM, 128-QAM, and 256-QAM. Note that the y-axis is in logarithmic scale. The results shown are averaged over 1000 simulation runs.

roughly 9 dB. During the tracking phase, a total of 1127 QAM-symbol errors in 1000 simulation runs (or equivalently, an average of 1.127 QAM symbol errors) occur.

For 256-QAM with an SNR margin of 3 dB, blind tracking results in a small SNR improvement ($\approx$ 1 dB). For subchannels with such low SNR margin, tracking might not be justifiable.

Note that the reason for the residual SNR loss after tracking is twofold: First, erroneous decisions during tracking cause an error bias. Second, the achievable SNR with vectoring for the channel $\boldsymbol{O}$ can be lower than for the channel $\boldsymbol{T}$.

3.5 CONCLUSION

Termination changes on alien lines can cause a serious degradation of receive SNR on lines operating wideband vectoring. Measurements and analysis show that while the impact is fairly mild for lower frequencies (below 20 MHz), an SNR-loss of up to around 15 dB can happen for higher frequencies. Maintaining retrain-free transmission with low SNR margins in case of such a termination-change event is a challenge.

Decision-directed channel tracking based on least-squares estimation can yield a fast and substantial SNR improvement in upstream direction without

losing spectral efficiency. In principle, blind channel tracking can also be used in downstream direction but requires fast feedback of the errors computed by the modems via subcarriers with high SNR margins to the distribution point during the upstream portions of TDD frames. Alternatively, a fast pilot-based channel-update mechanism could be introduced in order to avoid neighborhood wars.

ACKNOWLEDGMENT

This work was partly supported by the Swedish Research Council (VR) through grant No. 621-2007-6309 and by the Swedish Foundation for Strategic Research (SSF) through grant No. ICA08-0022.

References

[1] *Self-FEXT Cancellation (Vectoring) for Use with VDSL2 Transceivers*, International Telecommunication Union Recommendation, Sep. 2010.

[2] V. Oksman, H. Schenk, A. Clausen, J. M. Cioffi, M. Mohseni, G. Ginis, C. Nuzman, J. Maes, M. Peeters, K. Fisher, and P.-E. Eriksson, "The ITU-T's new G.vector standard proliferates 100 Mb/s DSL," *IEEE Communications Magazine*, vol. 48, no. 10, pp. 140–148, Oct. 2010. [Online]. Available: http://dx.doi.org/10.1109/MCOM.2010.5594689

[3] P. Ödling, T. Magesacher, S. Höst, P. Börjesson, M. Berg, and E. Areizaga, "The fourth generation broadband concept," *IEEE Communications Magazine*, vol. 47, no. 1, pp. 62–69, 2009.

[4] C. Lu and P.-E. Eriksson, "A fast channel estimation method for disorderly leaving events in vectored DSL systems," in *IEEE International Conference on Communications (ICC)*, 2011, pp. 1–6.

[5] *Self-FEXT Cancellation (Vectoring) for Use with VDSL2 Transceivers - Corrigendum 1*, International Telecommunication Union Recommendation, Jun. 2011.

[6] Sckipio, "Power saving implications on vectoring – static allocation case," ITU-T SG15 Contribution 2012-11-4A-043, Nov. 2012.

[7] Lantiq, "G.fast: Issues with discontinuous operation," ITU-T SG15 Contribution 2013-05-Q4-057, May 2013.

[8] ——, "G.fast: Precoder update in support of discontinuous operation," ITU-T SG15 Contribution 2013-01-Q4-068, Jan. 2013.

[9] Alcatel-Lucent, "G.fast: Solutions for precoding in discontinuous operation," ITU-T SG15 Contribution 2013-03-Q4-052, Mar. 2013.

[10] TNO, "G.fast: Vectoring gain limitations due to changing terminations of alien wire pairs," ITU-T SG15 Contribution 2013-03-Q4-044, Mar. 2013.

[11] R. Cendrillon, G. Ginis, E. Van den Bogaert, and M. Moonen, "A near-optimal linear crosstalk canceler for upstream VDSL," *IEEE Transactions on Signal Processing*, vol. 54, no. 8, pp. 3136–3146, 2006.

[12] ——, "A near-optimal linear crosstalk precoder for downstream VDSL," *IEEE Transactions on Communications*, vol. 55, no. 5, pp. 860–863, 2007.

[13] G. Marrocco, M. Wolkerstorfer, T. Nördstrom, and D. Statovci, "Energy-efficient DSL using vectoring," in *IEEE Global Telecommunications Conference (GLOBECOM)*, 2011, pp. 1–6.

[14] Lantiq, Broadcom, and Ikanos, "G.fast: Proposal for the transmit signal power limit," ITU-T SG15 Contribution 2012-06-4A-047R1, Jun. 2012.

4

Modeling Alien-Line Impedance-Mismatch in Wideband Vectored Wireline Systems

Eduardo Medeiros, Thomas Magesacher, Per Ödling, Dong Wei, Xiang Wang, Qiaojie Li, Per-Erik Eriksson, Chenguang Lu, Jeroen Boschma, and Bas van den Heuvel

Abstract

Sudden changes of channel coefficients in a wideband vectored wireline system (such as G.fast) due to changes in the terminating impedance of lines *outside* the vectored group can seriously degrade stability and throughput. This work presents a model that predicts the impact of termination mismatch based exclusively on crosstalk data for the properly-terminated state. Experimental results confirm a tight fit between model and measurements. The model allows analysis of system performance and stability without dedicated crosstalk measurements for mismatch cases.[1]

[1]Published in *IEEE Communications Letters*, vol. 18, no. 9, September 2014.

4.1 INTRODUCTION

Exploiting higher bandwidth on shorter copper loops, wireline access providers can provide higher throughput at reasonable deployment costs [1]. The draft ITU-T standard G.fast [2], for example, targets loop lengths in the order of 100 m using bandwidths in the order of 100 MHz to obtain aggregate[2] throughputs in the order of 1 Gbit/s. A key ingredient to achieving this performance is canceling far-end-crosstalk (FEXT) through techniques referred to as vectoring [3].

As bandwidths grow, termination mismatch has more and more impact on the performance of wideband vectoring systems. In practice, a termination mismatch on the customer premises (CP) side occurs when users turn off or disconnect their equipment or simply pick up their phones. At the other end, frequently referred to as distribution point (DP), a termination mismatch may—although probably less frequently—be caused by imperfect maintenance.

Measurements of termination mismatch and evaluation of the corresponding impact on performance have been presented in [4–7] and [8], respectively. A related issue are termination mismatches that occur inside the vectored group when modems leave (are turned off or being disconnected). This type of event, called a Disorderly Leaving Event (DLE) can be dealt with by quickly muting transceivers [9] or by executing a fast channel estimation procedure [10] [11].

Fig. 4.1 illustrates the degradation of signal-to-noise-power ratio (SNR) for a vectored G.fast user when changing the termination of a single *alien line* (a line outside the target vectored group). For many tones, the loss in SNR is far beyond 6 dB, which is the safety margin traditionally used by wireline operators to account for non-stationary channel effects. Simply increasing the SNR margin results in unacceptable throughput losses. Note that contrary to the DLE case, muting transceivers does not solve the problem. Furthermore, since the entire channel matrix is affected, tracking channel coefficients with error sample feedback takes considerable time.

In order to study this effect and assess its impact, accurate and comprehensive measurements are required. Direct measurement of crosstalk paths for each mismatch case is tedious and time-consuming. In this work, we present a model that allows us to predict the impact of impedance changes on crosstalk coupling paths using only crosstalk information for the all-terminated case. The latter is often a priori available, can be measured during an initialization phase where all lines are properly terminated, or can be extracted from established models.

[2]Sum of upstream and downstream bitrates.

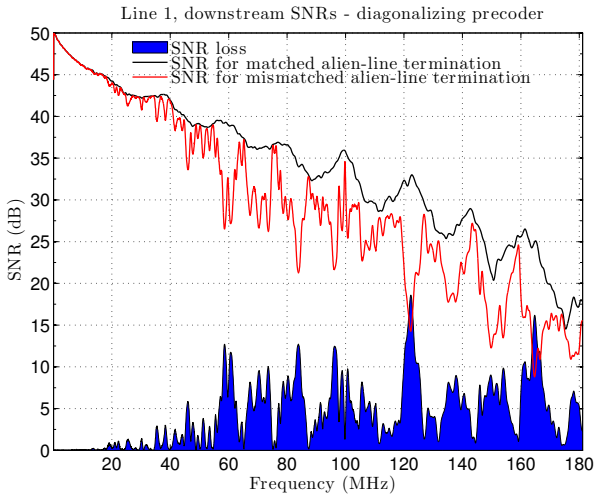

Figure 4.1: Impact of alien-line impedance mismatch: the drop in receive SNR (shaded blue area) when changing the alien-line termination from $100\,\Omega$ (solid black line) to open (solid red line) can be significant. (example for line no. 1 in a 2-line vectored group transmitting over a 100 m 30-pair cable).

Section 4.2 introduces the model and Section 4.3 provides an experimental verification showing a tight fit between directly measured and modeled crosstalk paths for the mismatch case. Section 4.4 demonstrates the application of the model to SNR predictions. Section 4.5 describes the main error sources and Section 4.6 concludes the work.

4.2 PROPOSED MODEL

Consider a wireline channel (cable) with M pairs. The two sides (cable ends) are hereinafter referred as DP-end and CP-end. The formulation presented here is valid for a single sub-carrier in the frequency domain. Let $H_{i,j}$ denote[3] the coupling coefficient between pair $j \in \{1,\ldots,M\}$ on the DP-end and pair $i \in \{1,\ldots,M\}$ on the CP-end. $H_{i,i}$ and $H_{i,j}, i \neq j$ thus denote direct channel coefficients and FEXT coupling coefficients in downstream direction, respectively. Let $N_{i,j}$ denote the coupling coefficient between pair $j \in \{1,\ldots,M\}$ on

[3]Notation: $H_{i,j}$ denotes the element in row no. i and column no. j of the matrix H and $H_{m:n,k:\ell}$ denotes the size $(n-m+1)\times(\ell-k+1)$ submatrix consisting of rows no. m to n and columns no. k to ℓ.

the CP-end and pair $i \in \{1, \ldots, M\}$ on the CP-end. $N_{i,i}$ and $N_{i,j}, i \neq j$ thus denote echo coefficients and near-end crosstalk (NEXT) coupling coefficients on the CP-end, respectively.

For illustration, but without loss of generality, we consider a small vectored group involving only two pairs no. 1 and no. 2 (cf. Fig. 4.2 top). In case all $2M$ termination impedances match perfectly, the receive signal on pair 1 at the CP-end can be written as

$$y_1 = H_{1,1}x_1 + H_{1,2}x_2, \tag{4.1}$$

where x_i are the transmit signals sent on the DP-end. Now assume that alien line no. ℓ, $\ell \in \{3, \ldots, M\}$ is terminated in a mismatching impedance on the CP-end, which results in a reflection of the arriving signal (cf. Fig. 4.2 bottom). Let $r_\ell \in \mathbb{C}, |r_\ell| \leq 1$ represent the reflection coefficient—ratio of reflected and arriving signal at the CP-end of line no. ℓ. The receive signal can then be written as

$$y_1 = \underbrace{(H_{1,1} + N_{1,\ell} r_\ell H_{\ell,1})}_{\hat{H}^O_{1,1}} x_1 + \underbrace{(H_{1,2} + N_{1,\ell} r_\ell H_{\ell,2})}_{\hat{H}^O_{1,2}} x_2. \tag{4.2}$$

Extending the idea to the general case of a vectored group over pairs[4] no. $1, \ldots, U$, the coupling coefficients for an arbitrary number of mismatched alien lines $\ell \in \mathcal{A} \subset \{U+1, \ldots, M\}$ are given by

$$\hat{H}^O_{1:U,1:U} = H_{1:U,1:U} + \sum_{\ell \in \mathcal{A}} r_\ell N_{1:U,\ell} H_{\ell,1:U} \tag{4.3}$$

In (4.3), we neglect second (and higher) order reflections. In other words, we do not consider components that couple into the vectored group after being reflected twice (or more often) at mismatched alien lines. To summarize, the model yields an estimate $\hat{H}^O$ of the coupling matrix H^O with alien-line termination mismatch[5] using *only* the coefficients H and N for the all-matched case and the reflection coefficient r_ℓ.

4.3 EXPERIMENTAL VERIFICATION

The experimental setup corresponds to the scenario depicted in Fig. 4.2. Three lines were chosen randomly from the same binder of a 0.5 mm, 100 m, 30-pair

[4] For clarity of notation we pick pairs no. 1 to U. Note that an arbitrary size-U set of pairs can be chosen out of $\{1, \ldots, M\}$ by renumbering the pairs.

[5] Although probably less likely, the dual scenario (i.e., training happens while there is an alien-line impedance mismatch and the change occurs when the matching impedance is connected) is possible and can be analyzed by the model.

cable [12]. Two pairs constitute a vectored group ($U = 2$). The third pair ($\ell = 3$) is used as the alien line. All remaining pairs were terminated in 100 Ω resistors.

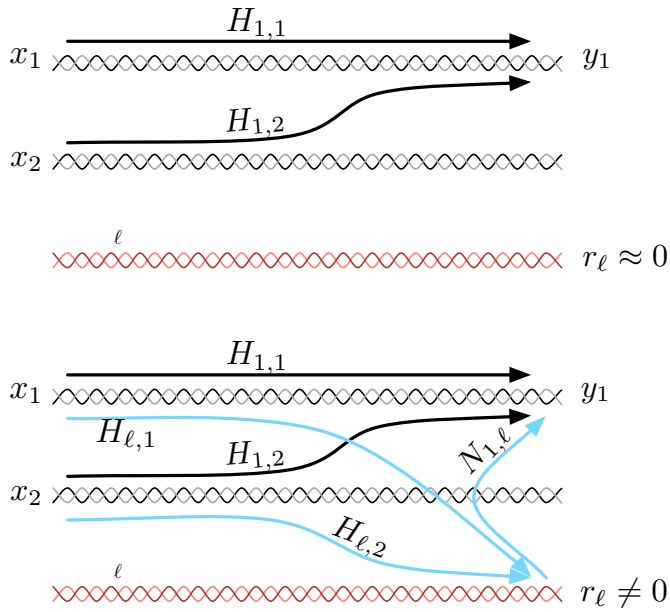

Figure 4.2: Illustration of the model's idea for downstream coupling in line no. 1. Top: For proper alien-line termination ($r_\ell \approx 0$), the received signal is simply $y_1 = H_{1,1}x_1 + H_{1,2}x_2$. Bottom: For alien-line termination mismatch ($r_\ell \neq 0$), the components $H_{\ell,1}x_1 + H_{\ell,2}x_2$ arriving at the mismatched port are reflected and yield an additional FEXT component $N_{1,\ell}r_\ell H_{\ell,1}x_1 + N_{1,\ell}r_\ell H_{\ell,2}x_2$ through the NEXT coupling path.

Direct gain/phase measurements for the approximately matched alien-line case $r_\ell \approx 0$ (Fig. 4.2 top) and the open alien-line case[6] $r_\ell = 1$ (Fig. 4.2 bottom) yield the matrix elements for H and H^O, respectively. In order to verify the model, $\hat{H}^O$ given by (4.3) is calculated from all-terminated FEXT and all-terminated NEXT measurements as

$$\hat{H}^O = H_{1:2,1:2} + r_\ell N_{1:2,3} H_{3,1:2}. \tag{4.4}$$

[6]This choice of reflection coefficient is used to model the case where the customer premises equipment (CPE) is physically disconnected from the phone outlet.

The squared channel gains from line 2 into line 1 are shown in Fig. 4.3. In general, there is a good match between the directly measured coupling function $H_{1,2}^{O}$ (black line) and the modeled coupling function $\hat{H}_{1,2}^{O}$ (red line). The error is concentrated around some dips on the higher frequencies (> 100 MHz).

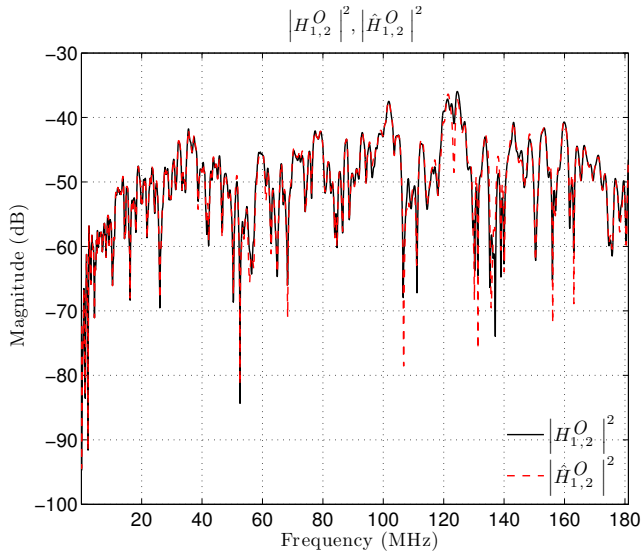

Figure 4.3: Squared magnitude of FEXT coupling coefficients from line 2 into line 1 with open alien line: direct measurement $H_{1,2}^{O}$ and calculated coupling path $\hat{H}_{1,2}^{O}$ using the proposed model (4.3).

4.4 APPLICATION

In order to demonstrate the virtues of the proposed model, the channel data is now used to calculate the SNR when utilizing a diagonalizing precoder [13]. The upper and lower plot in Fig. 4.4 present results for vectored line no. 1 and no. 2, respectively. The reference SNR curves (black solid lines) labeled SNR_u, where u denotes the line number, were obtained by performing a precoding operation with perfect channel knowledge.

The curves in solid red lines, labeled SNR_u^O, represent the SNR obtained after the alien line termination is removed, resulting in outdated precoder settings. The areas shaded in yellow, denoted ΔSNR_u, represent the SNR loss caused by the termination change. They are calculated as follows

$$\Delta SNR_u = SNR_u - SNR_u^O.$$

The curves in solid blue lines, labeled $\widehat{SNR}_u^O$ were obtained using the channel matrix $\hat{H}^O$ obtained by the model proposed in this letter. It is possible to observe a tight fit between SNR_u^O and $\widehat{SNR}_u^O$ throughout the considered frequency bands.

Finally, the error $e_u = \widehat{SNR}_u^O - SNR_u^O$, is depicted as the area shaded in magenta. It is possible to observe that the error in SNR caused by assuming the proposed model peaks at around 3.3 dB for line 1 and at 2.5 dB for line 2. For both lines, the error could be comfortably covered by the commonly adopted 6 dB of SNR margin.

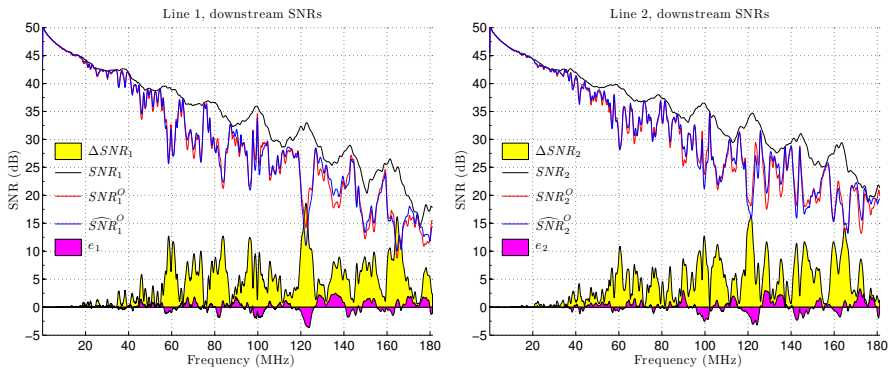

Figure 4.4: SNR comparison before and after the alien-line termination change using diagonalizing precoding in downstream direction, for lines 1 (top) and 2 (bottom). The black line represents SNR_u, the SNR before alien line termination change. The red lines represents SNR_u^O, the SNR after the terminating resistor is removed. The area shaded in yellow represents ΔSNR_u. The shaded area in magenta represents the SNR error between measurement data and the proposed model.

4.5 ERROR SOURCES

A small discrepancy between unterminated channel measurements, H^O, and channel estimates $\hat{H}^O$ obtained from the proposed model can be observed in Fig. 4.3. This discrepancy is responsible for the error term e_u in the diagonalizing precoder performance presented in Fig. 4.4. In this section we describe the error sources that contribute to the mismatch between direct measurements and model estimates.

4.5.1 MEASUREMENT ERROR

The precision of the measurements for H, H^O and N is limited by the accuracy of the measurement equipment. According to the network analyzer manufacturer [14], its dynamic magnitude and phase accuracy is in the range of $\pm 0.05\,\mathrm{dB}$, ± 0.3 degree respectively.

For some of the measurement sets, the authors had to modify the setup (for example, by connecting and disconnecting terminating resistors manually, i.e. Fig. 3). Even the slightest change in cable geometry caused by such actions (like, for example, slightly bending a wire while dis-/reconnecting) can impact directly measured crosstalk results. Finally, one should also consider imperfect calibration as a source of error in the measurement process.

4.5.2 REFLECTION COEFFICIENT

A second source of error is the assumption of $r_\ell = 1$ for the open-circuit measurements. Since there is always a stray capacitance between the wire ends, r_ℓ is frequency dependent and decreases the termination impedance as frequency grows.

4.5.3 SECOND-ORDER REFLECTIONS

The unavoidable impedance mismatch between a CPE's resistive termination and the characteristic impedance of their respective copper pair results in a small value for the reflection coefficient. If in addition to the alien line one or more other line(s) are not terminated in their exact characteristic impedance ($r_k \neq 0, k \in \{1,\ldots,M\}\backslash\ell$), reflections occur which are not considered in the model. For example, assume $r_2 \neq 0$ in the three-line example (cf. Fig. 4.5). Signal components arriving at this port are reflected and cause an additional contribution to y_1 via $N_{1,2}$ both before ($r_\ell = 0$) and after ($r_\ell \neq 0$) an alien-termination mismatch occurs. For alien-line mismatch ($r_\ell \neq 0$), there is thus an additional term $N_{1,2} r_2 N_{2,\ell} r_\ell H_{\ell,k}$ in $\hat{H}^O_{1,k}$, which is not included in the model (4.3). We refer to this contribution caused by two reflections as second-order reflection.

Note that even for the simple three-line case there are reflections of infinite order between line 2 and line ℓ, however, they vanish due to NEXT coupling attenuation. In practical deployments, due to the distance between cable terminations (and consequently lower NEXT) higher order reflections can be safely disregarded. However, second-order reflections may result in a small modeling error.

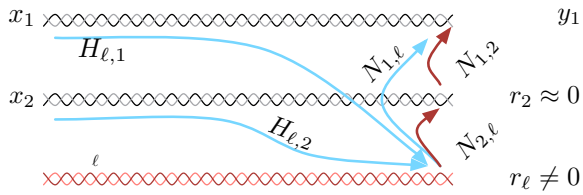

Figure 4.5: Example of second order reflection. The residual crosstalk received by line no. 1 due to a termination change in alien line ℓ is composed of a first-order reflection term (blue arrows) plus a second order reflection (red arrows), $N_{1,2}r_2N_{2,\ell}r_\ell\left(H_{\ell,1}x_1 + H_{\ell,2}x_2\right)$.

4.6 CONCLUSION

An impedance change on an alien line can cause significant changes in the channel matrix seen by a vectored group. Sudden changes may thus cause serious performance degradation or even system instability. In order to properly analyze the impact of this effect and develop appropriate counter measures, accurate and comprehensive channel data is required. Direct measurement of channel matrix changes caused by alien-line termination changes is cost- and labour-intensive. This letter proposes a model-based approach to capturing the impact of alien-line termination changes using only NEXT/FEXT data for the terminated case: based on NEXT/FEXT channel data, the signal arriving at the mismatched port is quantified. The mismatch causes a (possibly partial) reflection depending on the actual termination at hand. Using NEXT/FEXT channel data, the strengths of these components arriving at all ports of interest in the vectored group can be accurately computed.

References

[1] P. Ödling, T. Magesacher, S. Höst, P. Börjesson, M. Berg, and E. Areizaga, "The fourth generation broadband concept," *IEEE Communications Magazine*, vol. 47, no. 1, pp. 62–69, 2009.

[2] *Fast Access to Subscriber Terminals - Physical Layer Specification*, International Telecommunication Union Recommendation Draft, 2013.

[3] G. Ginis and J. Cioffi, "Vectored transmission for digital subscriber line systems," *IEEE Journal on Selected Areas in Communications*, vol. 20, no. 5, pp. 1085–1104, 2002.

[4] TNO, "G.fast: Vectoring Gain Limitations due to Changing Terminations of Alien Wire Pairs," ITU-T SG15 Contribution 2013-03-Q4-044, Mar. 2013.

[5] Lund University and Ericsson AB, "G.fast: Impact of Alien-Line Termination Changes on Vectoring Performance," ITU-T SG15 Contribution 2013-10-Q4-028, Oct. 2013.

[6] Alcatel-Lucent, "G.fast: Influence of an Impedance Change on a Leaving Line onto the Direct and Crosstalk Channels of the Active Lines," ITU-T SG15 Contribution 2013-10-Q4-058, Oct. 2013.

[7] Futurewei Technologies, "G.fast: SNR Drop and FEXT Channel Variations due to Change of Alien Termination," ITU-T SG15 Contribution 2013-10-Q4-046, Oct. 2013.

[8] E. Medeiros, T. Magesacher, P.-E. Eriksson, C. Lu, and P. Ödling, "How vectoring in G.fast may cause neighborhood wars," in *Proc. IEEE International Conference on Communications (ICC)*, 2014, pp. 3865–3870.

[9] *Self-FEXT Cancellation (Vectoring) for Use with VDSL2 Transceivers*, International Telecommunication Union Recommendation, Sep. 2010.

[10] C. Lu and P.-E. Eriksson, "A fast channel estimation method for disorderly leaving events in vectored DSL systems," in *Proc. IEEE International Conference on Communications (ICC)*, 2011, pp. 1–6.

[11] *Self-FEXT Cancellation (Vectoring) for Use with VDSL2 Transceivers - Corrigendum 1*, International Telecommunication Union Recommendation, Jun. 2011.

[12] Ericsson AB, *Access Network Pair cable, TEL 312*, 2010. [Online]. Available: http://goo.gl/4RdCXc

[13] R. Cendrillon, G. Ginis, E. Van den Bogaert, and M. Moonen, "A near-optimal linear crosstalk precoder for downstream VDSL," *IEEE Transactions on Communications*, vol. 55, no. 5, pp. 860–863, 2007.

[14] Agilent Technologies, Inc., *Agilent 4395A Network/Spectrum/Impedance Analyzer 500 MHz*, 2000. [Online]. Available: http://goo.gl/suqFrM

5

Mitigating Disorderly Leaving Events in G.fast

Yezi Huang, Thomas Magesacher, Eduardo Medeiros,
Chenguang Lu, Per-Erik Eriksson and Per Ödling

Abstract

Vectoring is a vital component of wideband wireline communication systems. A disorderly leaving event (DLE) disturbs the vectoring operation since the precoder, which was designed for the channel before the change, is no longer up to date. Measurements indicate that the impact of a DLE can be serious for frequencies beyond 30 MHz, which corresponds to the band used by emerging wideband communication systems over short multi-pair copper cables such as G.fast. As an alternative to the state-of-the-art update procedure, this paper presents an approach to mitigating the DLE problem. By interpreting DLE with the FEXT-reflected-NEXT (FRN) model, we propose a scheme that enables the showtime lines to return to disturbance-free transmission once the loss of signal on a certain line is detected while updating the precoder as a background process. Furthermore, the estimation complexity for a K-user vectoring group is reduced from $\mathcal{O}(K^2)$ to $\mathcal{O}(K)$. [1]

[1]Published in *Proc. IEEE International Conference on Communications (ICC 2015)*, London, United Kingdom, 08-12 Jun. 2015.

5.1 INTRODUCTION

The widespread deployment of cloud-based services and video-on-demand offerings continues to drive data rate and quality of service requirements for last-mile connections. In response to this trend, the wireline access industry advances towards a fiber to the last distribution point paradigm [1]. In this scenario, the recently consented G.fast standard [2] exploits shorter copper pairs and high bandwidth to provide up to around 1 Gbits/s aggregate net data rate.

Modern wideband wireline communication systems (such as G.fast) employ techniques referred to as vectoring [3] in order to cooperatively mitigate crosstalk. As vectoring relies on accurate channel information, changes of the terminating impedance in the multi-port wireline channel may cause severe performance degradation in terms of signal-to-noise ratio (SNR) as exemplified in Fig. 5.1. A change of impedance alters the perceived channel coupling conditions, and leads to residual crosstalk caused by an outdated precoder (or equalizer).

A particular event resulting in sudden termination change occurs when a modem *within* an active vectored group is turned off abruptly or is disconnected due to line disruption. This occurrence is called a disorderly leaving event (DLE), and was first reported during the development of vectored VDSL2 [3]. A fast channel tracking method was proposed in [4] to deal with DLEs in VDSL2. Unfortunately, it cannot be applied to G.fast since it is based on the assumption that only one column of the channel matrix changes.

In [5], a procedure is described that allows G.fast transceivers to leave a vectored group without negatively impacting the performance of other lines in the same bundle. The main idea is to allow coordination between transceivers at both ends, and acquire information necessary to update the precoder/equalizer before the line leaves and its termination impedance changes. While solving the problem of orderly leaving events, [5] does not address situations where there is no previous intent announced by the leaving transceiver(s).

This paper has two main contributions: First, we extend the model presented in [6] [7] to address DLEs, and identify the source of DLE disturbance that we can control. Second, we develop a novel precoder update procedure that does not disturb other lines while performing channel estimation as a background process.

The paper is organized as follows. In Section 5.2 a system model is presented to explain DLE. Taking advantage of this model, we formulate the DLE disturbance in Section 5.3 and propose in Section 5.4 a parameter-based channel estimation procedure that minimizes the impact of DLEs for the remaining active users. Section 5.5 demonstrates the effectiveness of the proposed method with channel measurements and simulations. Section 5.6 concludes

the work.

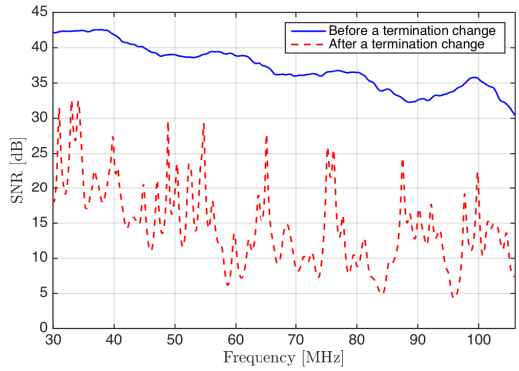

Figure 5.1: SNR on one victim line before and after a termination change. The SNR drop represents the impact of a disrupted vectoring.

Notation: Bold capital letters (*e.g.*, $\mathbf{A}$) and bold lower-case letters (*e.g.*, $\mathbf{a}$) denote matrices and column vectors, respectively. $a_{i,j}$ is an element on the i-th row and j-th column of $\mathbf{A}$ and a_i is the i-th element of $\mathbf{a}$. $\mathbf{I}_{n\setminus i}$ is an n-dimensional identity matrix excluding the i-th row. $\mathcal{M}_i\{\mathbf{A}\}$ denotes an operator deleting both the i-th row and column from $\mathbf{A}$. Operator "$\setminus$" excludes certain element(s) on the right-hand side from the set on the left-hand side.

5.2 FEXT-REFLECTED-NEXT (FRN) MODEL FOR DLE

Consider a wideband discrete multi-tone modulation (DMT) system with a group of K twisted pairs (or equivalently, users). The twisted pairs connect the transceivers at the distribution point (DP) with the customer premise equipment (CPE).

In [6] [7], a FEXT-reflected-NEXT (FRN) model is proposed to characterize the changed coupling condition due to an alien-line impedance mismatch at the CPE. A DLE is similar—except now the impedance change happens within the vectored group as illustrated in Fig. 5.2. Without loss of generality, we illustrate the DLE coupling model in downstream on a certain sub-carrier. Since G.fast employs Time–Division Duplex (TDD), the model for downstream applies, *mutatis mutandis*, to upstream.

Let $\mathbf{H} \in \mathbb{C}^{K\times K}$ denote the frequency-domain channel matrix on a certain sub-carrier for the perfectly-terminated case, where diagonal and off-diagonal elements are direct-channel coefficients and far-end crosstalk (FEXT) coefficients, respectively. For the sake of simple notation, but without loss of gener-

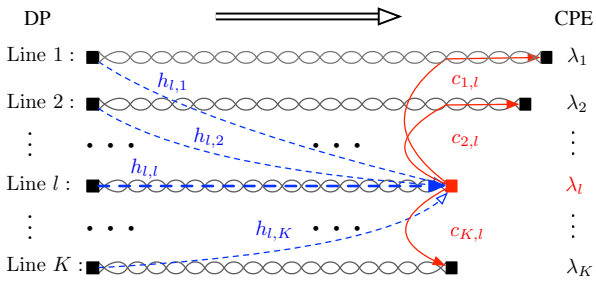

Figure 5.2: Downstream FRN model. *Dash lines*: Channel paths from DP to the mismatched termination l. *Solid lines*: near-end coupling paths from the mismatched termination l to the remaining CPEs.

ality, the sub-carrier index is omitted. Let $\mathbf{\Lambda} = \text{diag}([\lambda_1, \lambda_2, \ldots, \lambda_K]) \in \mathbb{C}^{K\times K}$ denote a diagonal matrix with termination reflection coefficients and let $\mathbf{C} \in \mathbb{C}^{K\times K}$ denote the near-end crosstalk (NEXT) coupling matrix at the CPE-side. For scenarios with unequal pair-lengths, $\mathbf{C}$ denotes attenuated NEXT (as illustrated in Fig. 5.2 for the l-th column of $\mathbf{C}$). The diagonal entries of $\mathbf{C}$, corresponding to the CPE-side echo coefficients, are assumed to be 0. The channel matrix $\mathbf{H}'$ for the general case is

$$\mathbf{H}' = \mathbf{H} + \mathbf{\Delta},$$

where $\mathbf{\Delta} = \mathbf{C\Lambda H}$ quantifies the deviation from the all-terminated case according to the FRN model. When the terminations at the CPE are perfectly matched (*i.e.*, $\lambda_i = 0$ for $i = 1, \ldots, K$), then $\mathbf{\Delta} = \mathbf{0}$ and thus $\mathbf{H}' = \mathbf{H}$.

Vectoring enables cooperative signal processing within the group. A properly designed precoder in downstream and equalizer in upstream at the DP significantly reduces FEXT. In this work, we focus on linear precoding and thus on the frequency range up to 106 MHz (cf. [2]). Specifically in downstream, let $\mathbf{G} = \text{diag}([g_1, g_2, \ldots, g_K]) \in \mathbb{R}^{K\times K}$ denote a diagonal matrix with the gain adjusters for each line on the main diagonal. Assume that the cyclic prefix of DMT is not shorter than the impulse responses of the coupling paths. Furthermore, assume that the inverse fast Fourier transform (IFFT) for the group users is well synchronized. After including linear precoder $\mathbf{P}_o$, transmitting $\mathbf{x} \in \mathbb{C}^{K\times 1}$ at the DP-side yields the receive signal $\mathbf{y} \in \mathbb{C}^{K\times 1}$ given by

$$\mathbf{y} = \mathbf{H}'\mathbf{P}_o\mathbf{G}\mathbf{x} + \mathbf{n},$$

where $\mathbf{n} \in \mathbb{C}^{K\times 1}$ denotes the background noise. An ideal precoder designed for $\mathbf{H}$ at DP neutralizes the crosstalk effectively such that for the input symbols

x

$$\mathbf{H}\mathbf{P}_o\mathbf{G}\mathbf{x} = \mathbf{\Sigma}\mathbf{x}, \tag{5.1}$$

where $\mathbf{\Sigma} \in \mathbb{C}^{K\times K}$ is diagonal.

In practice, most often only one diagonal element of $\mathbf{\Lambda}$ will deviate significantly from 0 as a result of a DLE (*i.e.*, mismatch of a single line only). Assume line l exhibits a DLE, which is quantified by a reflection coefficient $|\lambda_l| \gg 0$. Consequently, $\mathbf{\Delta} \neq \mathbf{0}$ and all FEXT coupling coefficients change. The new FEXT arriving at termination k, $(k \neq l)$ is determined by

$$(\mathbf{h}'_k)^T = \mathbf{h}_k^T + c_{k,l}\lambda_l\mathbf{h}_l^T,$$

where $\mathbf{h}_l^T$ indicates the l-th row of $\mathbf{H}$, and $(\mathbf{h}'_k)^T$ is the k-th row of $\mathbf{H}'$. The outdated precoding with $\mathbf{P}_o$ fulfilling Eq. (5.1) yields the disturbed receive signal

$$\mathbf{y}' = \underbrace{\mathbf{H}\mathbf{P}_o\mathbf{G}\mathbf{x} + \mathbf{n}}_{\mathbf{y}_d} + \underbrace{\mathbf{C}\mathbf{\Lambda}\mathbf{H}\mathbf{P}_o\mathbf{G}\mathbf{x}}_{\boldsymbol{\xi}}, \tag{5.2}$$

where $\mathbf{y}_d$ is the desired receive signal obtained in the perfectly-terminated case and $\boldsymbol{\xi}$ is the residual crosstalk due to the DLE. Equivalently, the effective channel changes from $\mathbf{H}$ to $\mathbf{H}' = \mathbf{H} + \mathbf{\Delta}$.

The FRN model described in [6] [7] suggests that FEXT arrives at and is reflected by the alien mismatched termination only. Compared to the alien-line case, in a DLE the leaving line is always active. As the direct path $h_{l,l}$ has a lower channel attenuation than the FEXT paths $h_{l,k}$, $k \in \{1,\ldots,K\}\backslash l$, the residual-crosstalk issue in a DLE could be even worse.

We demonstrate the impact of a DLE on the channel coupling conditions by means of crosstalk-paths and direct-path measurements from a 30-pair, 100 m, 0.5 mm cable [8]. 10 pairs from a single binder were chosen at random. The measurement points follow a 51.75 kHz sub-carrier spacing, and we consider 2 048 sub-carriers in total corresponding to the frequency range up to 106 MHz. The all-terminated case and a DLE-case where line $l = 10$ is left unterminated yield two 10×10 matrices $\mathbf{H}$ and $\mathbf{H}'$ respectively. The 10-th row of $\mathbf{H}'$ is left the same as that of $\mathbf{H}$. The corresponding channel-matrix deviation is thus given by $\mathbf{\Delta} = \mathbf{H}' - \mathbf{H}$. We quantify the impact of this DLE on vectoring in terms of the worst residual crosstalk $\mathcal{P}_k^{\text{rx}}$ over all lines

$$\mathcal{P}_k^{\text{rx}} = \mathcal{P}^{\text{tx}} + 20\log_{10}(\max_i |\delta_{i,k}|), \tag{5.3}$$

when line k is excited by a signal with transmit power spectrum density (PSD) $\mathcal{P}^{\text{tx}}$. In essence, Eq. (5.3) evaluates the maximum power of the k-th column of $\mathbf{\Delta}$.

Fig. 5.3 shows the crosstalk power for $\mathcal{P}^{\text{tx}} = -76\,\text{dBm/Hz}$ with respect to the background noise of $-140\,\text{dBm/Hz}$. Clearly, the channel changes in

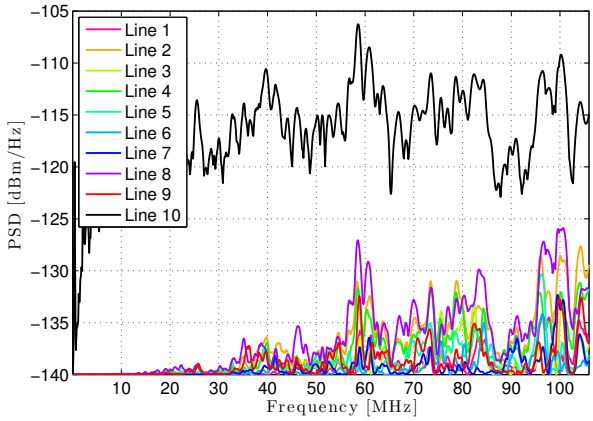

Figure 5.3: Comparison of the strongest crosstalk caused by each column of $\mathbf{\Delta}$, when having a vectored group size of $K = 10$ and line $l = 10$ is leaving.

the column $l = 10$ (black curve) are dominant, which is consistent with the assumption in [4]. However, channel changes in the other columns become disturbing for frequencies beyond 30 MHz. Except for the l-th row, every other entry of $\mathbf{\Delta}$ contributes to the new channel $\mathbf{H}'$. Equivalently, almost every element of $\mathbf{H}$ changes due to a DLE.

5.3 RESIDUAL CROSSTALK ANALYSIS

In downstream direction, changed channel coupling conditions result in an outdated precoder. Specifically, the linear precoder as in [9] defines

$$\mathbf{P}_o = \mathbf{H}^{-1}\mathbf{H}_\Sigma, \tag{5.4}$$

where the diagonal matrix $\mathbf{H}_\Sigma$ contains direct channel coefficients of the all-terminated channel $\mathbf{H}$.

Consider the DLE case where line l leaves while all other lines are perfectly terminated. Thus, $\mathbf{\Lambda} = \text{diag}\left([0,\ldots,0,\lambda_l,0,\ldots,0]\right)$ and the resulting reflection-followed-by-NEXT paths $\mathbf{C\Lambda}$ are given by

$$\mathbf{C\Lambda} = \begin{bmatrix}\mathbf{0} & \ldots & \mathbf{0} & \mathbf{v}_l & \mathbf{0} & \ldots & \mathbf{0}\end{bmatrix}, \tag{5.5}$$

where the reflecting crosstalk coefficients are defined in a vector as

$$\mathbf{v}_l = \lambda_l \left[c_{1,l},\ldots,c_{i,l},\ldots,c_{K,l}\right]^T. \tag{5.6}$$

According to Eq. (5.2), the residual crosstalk when using the outdated precoder $\mathbf{P}_o$ is given by

$$\begin{aligned}\boldsymbol{\xi} &= \mathbf{C}\boldsymbol{\Lambda}\mathbf{H}\mathbf{P}_o\mathbf{G}\mathbf{x} \\ &= \mathbf{C}\boldsymbol{\Lambda}\mathbf{H}_{\Sigma}\mathbf{G}\mathbf{x}. \end{aligned} \tag{5.7}$$

Using Eq. (5.5), the expression (5.7) for the residual crosstalk simplifies to

$$\begin{aligned}\boldsymbol{\xi} &= \mathbf{v}_l h_{l,l} g_l x_l \\ &= \mathbf{v}_l \sigma_l x_l, \end{aligned} \tag{5.8}$$

where x_l is the l-th element of $\mathbf{x}$, and $\sigma_l = h_{l,l}g_l$ is the effective gain for path l.

Eq. (5.8) reveals that retaining the outdated precoder $\mathbf{P}_o$ can eliminate the possible FEXT-reflected-NEXT components since the precoder keeps doing its job of mitigating/eliminating FEXT arriving at the reflective surface of termination l. The only source of the residual crosstalk $\boldsymbol{\xi}$ is the transmitted signal x_l on the leaving line via the l-th direct channel $h_{l,l}$ (see the bold dash line in Fig. 5.2), which is then reflected and couples to other CPEs via $\mathbf{v}_l$.

A traditional reaction to DLE, however, is to stop transmission on the leaving line as soon as possible, and quickly update the linear precoder at the DP to $\overline{\mathbf{P}}$ fulfilling

$$\mathcal{M}_l\left\{\mathbf{H}\right\}\overline{\mathbf{P}}\mathcal{M}_l\left\{\mathbf{G}\right\} = \mathcal{M}_l\left\{\boldsymbol{\Sigma}\right\}, \tag{5.9}$$

to diagonalize the dimension-reduced original channel $\mathcal{M}_l\left\{\mathbf{H}\right\}$. The FRN model implies that stopping transmission on the leaving line only avoids FEXT from line l (*i.e.*, the l-th column of $\mathbf{H}$), but does not avoid FEXT to line l (*i.e.*, the l-th row of $\mathbf{H}$). Instant update of the precoder to $\overline{\mathbf{P}}$ does not cancel FEXT through paths $h_{l,k}$ for $k \in \{1,\ldots,K\}\backslash l$, which are then reflected at mismatched port and couple as NEXT to the victim lines resulting in residual crosstalk. Moreover, immediate line shutoff is sensitive to DLE false alarm or detection failure [4], which leads to unnecessary retraining of the tranceivers.

In the upstream direction, the FRN model suggests that the leaving line l "emits" an unwanted upstream signal as a result of "incoming" NEXT being reflected by the mismatched port at the CPE side. The resulting upstream FEXT through coupling into $k \in \{1,\ldots,K\}\backslash l$ is taken care of by the interference canceler, whose coefficients are still correct for coupling paths from line l at the CPE to lines $k \in \{1,\ldots,K\}\backslash l$ at the DP. The resulting upstream FEXT coefficients from lines $k \in \{1,\ldots,K\}\backslash l$ into line l change and cause residual FEXT at the interference canceler output on line l, which is no problem since transmission on line l is interrupted anyway.

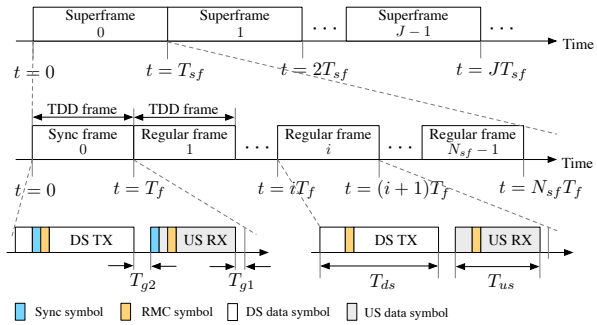

Figure 5.4: G.fast TDD structure at the DP-side. Time gaps are reserved between paired down- and up-stream as T_{g2} and between upstream and next downstream as T_{g1}. The sum of the T_{g1} and T_{g2} equals to one DMT symbol duration.

5.4 PROPOSED RESIDUAL-CROSSTALK-FREE CHANNEL ESTIMATION

A reference time-line for G.fast TDD frames is shown in Fig. 5.4. A typical TDD frame is $T_f = 750\,\mu s$ long and consists of $N_f = 36$ DMT symbols. A superframe for this setting consists of $N_{sf} = 8$ TDD frames. The first frame of each superframe is a sync-frame, which contains one synchronization symbol located at a predefined symbol position in both directions. The sync-frame is then followed by 7 regular frames without synchronization symbols.

Assume that a DLE happens at time instant t_l at the CPE. In case t_l falls into a downstream transmission interval of the i-th TDD frame ($t_l \in \big[(i-1)T_f, (i-1)T_f + T_{ds}\big]$), the DP will detect this event during the next upstream transmission period ($t \in \big[(i-1)T_f + T_{ds} + T_{g2}, iT_f - T_{g1}\big]$). The DP initiates upstream channel tracking and in the next downstream transmission period and onwards ($t \geq iT_f$), it transmits *idle symbols* [2] at non-synchronization symbol positions on the leaving line l. The main idea is to mute the data symbols on line l but keep transmitting the anti-crosstalk signals to cancel out FEXT arriving at the mismatched termination of line l at the CPE. According to the FRN model (cf. Fig. 5.2), there is thus no energy to cause reflections and subsequent NEXT into the other lines. A more detailed illustration for this special operation will be given below. If the DLE occurs during an upstream transmission interval, the channel tracking for upstream and "muting line l" for downstream launch directly.

Generally, instead of turning off the leaving line immediately after detecting a loss of signal (*los*), channel estimation and precoder update in downstream direction is accomplished by alternating two kinds of special symbols: idle symbols and synchronization symbols (as illustrated in Fig. 5.5).

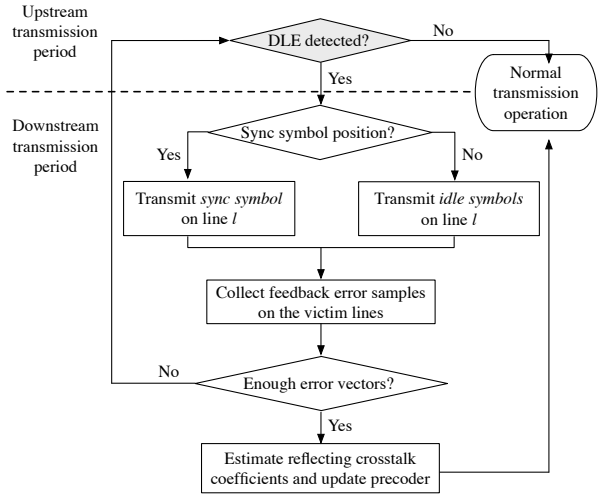

Figure 5.5: Flowchart of proposed operation at the DP-side

SILENT MODE By modifying the l-th gain adjuster to be $g_l = 0$ at non-synchronization symbol positions, idle symbols are transmitted on the leaving line. The residual crosstalk $\boldsymbol{\xi}$ in Eq. (5.8) on the victim lines becomes $\boldsymbol{\xi} = \mathbf{v}_l h_{l,l} x_l \cdot 0 = 0$. It enables "silent" estimation and updating in the sense that active users remain undisturbed. Thus, we call this kind of transmission mode *silent mode*. The DLE noisy period is at most $T_{ds} + T_{g2}$ before *los* on line l is detected.

SYNCHRONIZATION MODE Synchronization symbols are transmitted every 6 ms (*i.e.*, one superframe duration) on each line in G.fast. Assume J superframes are required before the estimation is completed. Let t_j be the time instant to transmit the j-th downstream synchronization symbol. In this specific time slot, the l-th gain adjuster is set back to g_l, which is used for transmission before DLE. According to Eq. (5.1), Eq. (5.2) and Eq. (5.8), transmitting synchronization symbol $\mathbf{s}(t_j) = [s_1(t_j), \ldots, s_l(t_j), \ldots, s_K(t_j)]^T$ yields

$$\begin{aligned}\mathbf{q}(t_j) &= \boldsymbol{\Sigma}\mathbf{s}(t_j) + \mathbf{v}_l \sigma_l s_l(t_j) + \mathbf{n} \\ &= \boldsymbol{\Sigma}\left(\mathbf{s}(t_j) + \mathbf{e}(t_j)\right),\end{aligned}$$

where $\mathbf{e}(t_j) = \boldsymbol{\Sigma}^{-1}\left(\mathbf{v}_l \sigma_l s_l(t_j) + \mathbf{n}\right)$. The synchronization error samples $\mathbf{I}_{K\setminus l}\mathbf{e}(t_j)$ on the victim lines are then fed back to the DP [2].

After sending the synchronization symbol at the scheduled time instant, the transmission on line l goes back to idle symbols for all non-synchronization

symbol positions. Keep on alternatively sending idle symbols and synchronization symbols on the leaving line until DP collects J error symbols on the victim lines as

$$\begin{aligned}\mathbf{E} &= \mathbf{I}_{K\backslash l}\left[\mathbf{e}(t_1), \mathbf{e}(t_2), \ldots, \mathbf{e}(t_J)\right] \\ &= \mathbf{I}_{K\backslash l}\boldsymbol{\Sigma}^{-1}\mathbf{v}_l\sigma_l\mathbf{s}_l^T + \mathbf{N},\end{aligned}$$

where $\mathbf{s}_l = \left[s_l(t_1), \ldots, s_l(t_J)\right]^T$ is the synchronization sequence transmitted on the leaving line l at t_j $(j = 1, \ldots, J)$, and $\mathbf{N} \in \mathbb{C}^{(K-1)\times J}$ is the equalized additive noise on victim lines for J synchronization time instants. The contributing reflecting crosstalk coefficients in Eq. (5.6) can be estimated by

$$\widehat{\mathbf{v}}_l = \frac{\mathcal{M}_l\left\{\boldsymbol{\Sigma}\right\}\mathbf{E}\mathbf{s}_l^*\left(\mathbf{s}_l^T\mathbf{s}_l^*\right)^{-1}}{\sigma_l}, \quad \widehat{\mathbf{v}}_l \in \mathbb{C}^{(K-1)\times 1}, \tag{5.10}$$

where $\mathbf{s}_l^*$ is the conjugate of $\mathbf{s}_l$. Although the full channel matrix of $\mathcal{M}_l\left\{\mathbf{H}\right\}$ is changed due to a single DLE, the estimation effort of the proposed method reduces from $(K-1)^2$ parameters to $K-1$ by modeling the changed coupling condition with reflecting crosstalk coefficients in $\mathbf{v}_l$.

During the whole process, the DP-side is still able to track the received signal power on line l. In case of, for example, a false alarm of DLE, no channel retraining is required and it is fast to get back to the normal transmission by a simple setting on g_l.

With $\mathbf{v}_l$ estimated, the precoder can be updated for the new channel matrix $\mathcal{M}_l\left\{\mathbf{H}'\right\}$ according to the FRN model, *i.e.*,

$$\widehat{\mathbf{P}} = \left(\mathcal{M}_l\left\{\mathbf{H}\right\} + \widehat{\mathbf{v}}_l\boldsymbol{\mathcal{E}}_l^T\mathbf{H}\mathbf{I}_{K\backslash l}^T\right)^{-1}\mathcal{M}_l\left\{\mathbf{H}'_\Sigma\right\}, \tag{5.11}$$

where $\boldsymbol{\mathcal{E}}_l$ is an elementary column vector with only 1 on the l-th position and 0s elsewhere.

5.5 SIMULATION RESULTS

In order to evaluate the proposed scheme, we consider a vectoring system with $K = 3$ users operating on the 100 m-cable [8] introduced in Section 5.2. A DLE occurs on line $l = 3$. We use G.fast system parameters [2] and focus on the frequency-range up to 106 MHz. The special silent mode we propose in Section 5.4 is appraised in terms of SNR drop, introduced in Fig.5.1. We also compare our operation with the traditional method both in frequency and in time based on the PSD of the resulting residual crosstalk.

Fig. 5.6 shows that the SNR drop caused by a DLE on the victim lines can be mitigated by setting the gain scaling factor of line l to zero, which would essentially solve the DLE problem. However, keeping the analog front-end

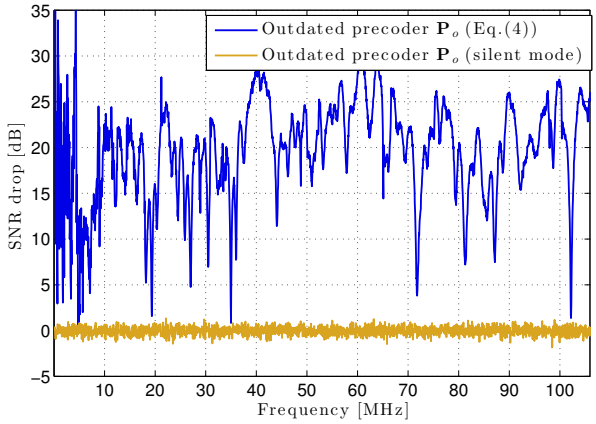

Figure 5.6: SNR drop on victim line 1 after DLE, given full line transmission with the outdated precoder $\mathbf{P}_o$.

running to send pure anti-crosstalk signals consumes power. If the line has already left, it is thus desirable to invoke the second mode in order to update the precoder for the new dimension-reduced channel $\mathcal{M}_l\{\mathbf{H}'\}$.

Fig. 5.7 presents the residual crosstalk PSD on one of the victim lines in the vectored group. By stopping transmission on the leaving line and updating the precoder to $\overline{\mathbf{P}}$ based on the dimension-reduced original channel $\mathcal{M}_l\{\mathbf{H}\}$ (*i.e.*, the traditional operation as defined by Eq. (5.9)), there is an improvement in SNR (comparing the second curve to the top one). However, the residual crosstalk power level is still far above the background noise level, especially for high frequencies where the crosstalk channel has a power level closer to that of the direct channel. Thus, further channel tracking is needed.

In contrast, both modes in our proposed operation suppress the residual crosstalk down to the background noise level throughout the studied frequency range. The victim lines are able to retrieve the residual-crosstalk-free transmission via the silent mode (yellow curve). With $J = 1$ synchronization symbol, the estimated precoder $\widehat{\mathbf{P}}$ can effectively take care of the new channel matrix $\mathcal{M}_l\{\mathbf{H}'\}$ (green curve).

Assume no persistent detection of *los* requirement as in [3] is considered for now, and no signal processing time is counted in. Fig. 5.8 and Fig. 5.9 compare the residual crosstalk on a certain sub-carrier when the DLE happens at two extreme time slots (time instants indicated by the black line): Fig. 5.8 shows the longest time distance to the next synchronization symbol, and Fig. 5.9 presents the shortest time distance. The average residual crosstalk power on

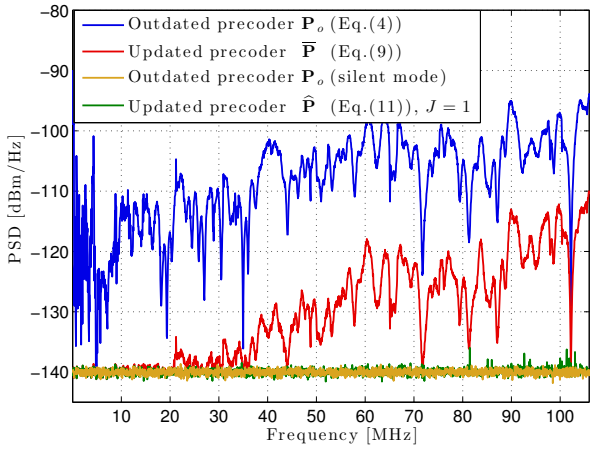

Figure 5.7: Residual crosstalk in frequency after DLE on victim line 1.

victim line k is calculated over one frame on one sub-carrier as

$$E[|\xi_k|^2] = \frac{1}{N_{ds}} \sum_{j=1}^{N_{ds}} |\xi_k(j)|^2,$$

where N_{ds} is the number of DMT symbols assigned to downstream transmission in one frame.

As indicated with different vertical time lines in Fig. 5.8 and Fig. 5.9, both the traditional and our proposed method deal with the DLE disturbance in two steps. Once *los* is detected, the first step is taken in the next frame (time instant marked by the yellow line). For the traditional method, the channel dimension is reduced and the precoder is updated to $\overline{\mathbf{P}}$. For our proposed method, the silent mode is activated by transmitting idle symbols on the leaving line. Both methods work well on low-frequency sub-carriers (*e.g.*, 20 MHz in Fig. 5.8a and Fig. 5.9a). However, on higher-frequency sub-carriers (*e.g.*, 100 MHz), $\overline{\mathbf{P}}$ is not adequate for crosstalk cancellation, as shown by the error plateau in Fig. 5.8b and Fig. 5.9b. Residual crosstalk severely disturbs the active users before enough error samples can be collected (time instant marked by the pink line) to proceed with a second step, aiming at a precoder update based on the acquired estimates. A traditional way is to perform an elementwise estimation of the dimension-reduced new channel $\mathcal{M}_l\{\mathbf{H}'\}$ using synchronization symbols and pilot sequences. When Hadamard sequences are applied, $2^{\lceil \log_2(K-1) \rceil}$ synchronization symbols are required to estimate $(K-1)^2$ channel matrix elements. For example, a single DLE in a vectored group of $K = 100$ would keep on disturbing the active users for at

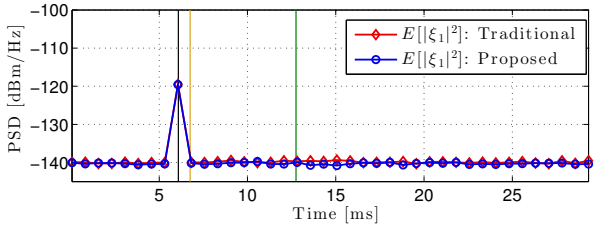

(a) Average residual crosstalk on a sub-carrier at 20 MHz

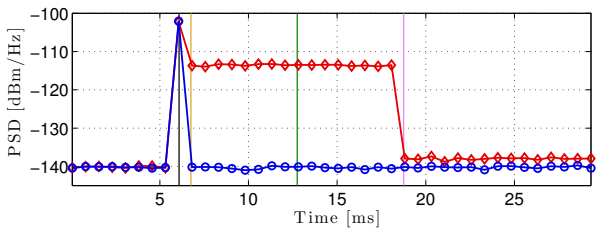

(b) Average residual crosstalk on a sub-carrier at 100 MHz

Figure 5.8: Average residual crosstalk $E[|\xi_1|^2]$ in time on victim line 1 in downstream at the worst situation: DLE happens one symbol after the synchronization symbol during downstream transmission interval.

least $128 \times 6 = 768$ ms, and require an estimation of $99^2 = 9\,801$ entries for each sub-carrier.

The proposed operation, instead, keeps residual crosstalk close to the background noise level during and after the process of estimation and update (time instant marked by the green line), and makes the dimension-reducing operation unnoticeable. Once the DP is aware of the *los*, there is no more crosstalk disturbing the victim lines. Given persistently detected *los* on line l and accomplished estimation of the new channel matrix, it is safe then to completely remove line l from the vectored group.

It is worth noting that keeping the precoder the same as before the DLE during channel estimation has three advantages. First, other active users in showtime are not disturbed, thanks to the silent mode. Second, it enables FRN-based modeling, which significantly reduces the estimation effort. A traditional method requires orthogonal synchronization sequences to estimate $(K-1)^2$ channel coefficients, while our parameter-based method can exploit the synchronization symbols on line l as a unique reference for estimating the $K-1$ reflecting coefficients only. Third, our estimation does not rely on

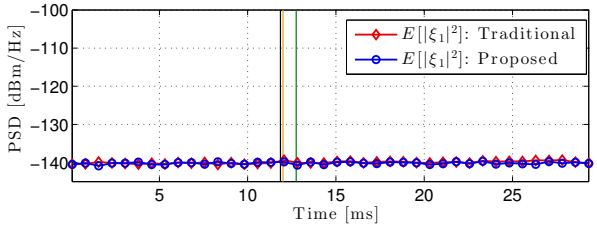

(a) Average residual crosstalk on a sub-carrier at 20 MHz

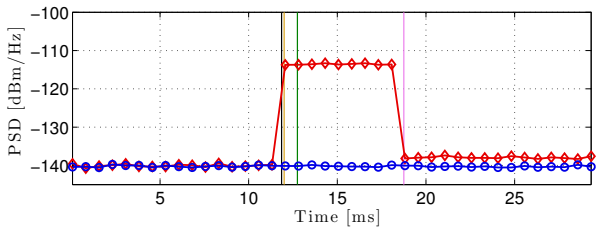

(b) Average residual crosstalk on a sub-carrier at 100 MHz

Figure 5.9: Average residual crosstalk $E[|\xi_1|^2]$ in time on victim line 1 in downstream at the best situation: DLE happens one frame before the synchronization frame during upstream transmission interval.

the orthogonality property. The traditional method shows a slightly higher residual crosstalk-PSD level on severely impacted sub-carriers (cf. Fig. 5.8b and Fig. 5.9b), since the required orthogonality is degraded by background noise.

5.6 CONCLUSION

A sudden termination change due to a DLE alters the original channel matrix of a vectored group, which can have serious consequences for the vectoring operation. Based on the FRN model, we identify the sources and paths for residual crosstalk after the DLE and introduce a model that is parameterized by reflecting crosstalk coefficients. A procedure for channel estimation and precoder update in the downstream direction is proposed. Temporarily retaining the outdated precoder after a DLE narrows potential residual crosstalk paths down to only the direct channel of the leaving line. Compared to the state-of-the-art method, the period during which active users are disturbed

can be significantly shortened to the time it takes to detect the loss of signal and the estimation complexity for a K-user system is reduced from $\mathcal{O}(K^2)$ to $\mathcal{O}(K)$.

References

[1] P. Ödling, T. Magesacher, S. Höst, P. Börjesson, M. Berg, and E. Areizaga, "The Fourth Generation Broadband Concept," *IEEE Communications Magazine*, vol. 47, no. 1, pp. 62–69, January 2009.

[2] ITU, "Fast Access to Subscriber Terminals - Physical Layer Specification," International Telecommunication Union Recommendation Draft, 2014.

[3] ——, "Self-FEXT cancellation (vectoring) for use with VDSL2 transceivers," Recommendation ITU-T G.993.5, Apr. 2010. [Online]. Available: https://www.itu.int/rec/T-REC-G.993.5/en

[4] C. Lu and P.-E. Eriksson, "A Fast Channel Estimation Method for Disorderly Leaving Events in Vectored DSL Systems," in *Proc. 2011 IEEE International Conference on Communications (ICC)*, June 2011, pp. 1–6.

[5] Alcatel-Lucent, "Influence of an Impedance Change on a Leaving Line onto the Direct and Crosstalk Channels of the Active Lines," ITU-T SG15 Contribution 2013-10-Q4-058, Oct. 2013.

[6] Futurewei Technologies, "G.fast: SNR Drop and FEXT Channel Variations due to Change of Alien Termination," ITU-T SG15 contribution 2013-10-q4-046, Mar. 2013.

[7] E. Medeiros, T. Magesacher, P. Ödling, D. Wei, X. Wang, Q. Li, P. Eriksson, C. Lu, J. Boschma, and B. van den Heuvel, "Modeling Alien-Line Impedance Mismatch in Wideband Vectored Wireline Systems," *IEEE Communications Letters*, vol. 18, no. 9, pp. 1527–1530, Sept 2014.

[8] Ericsson AB, *Access Network Pair cable, TEL 312*, 2010. [Online]. Available: http://goo.gl/4RdCXc

[9] R. Cendrillon, G. Ginis, E. Van den Bogaert, and M. Moonen, "A Near-Optimal Linear Crosstalk Precoder for Downstream VDSL," *IEEE Transactions on Communications*, vol. 55, no. 5, pp. 860–863, May 2007.

6

Enabling DSL and Radio on the Same Copper Pair

Yezi Huang, Eduardo Medeiros, Stefan Höst, Thomas Magesacher, Per-Erik Eriksson, Chenguang Lu, Per Ödling and Per Ola Börjesson

Abstract

To increase indoor coverage for mobile services, we propose a residential small cell infrastructure making use of the existing copper plant. The system is cabinet-based, collocated with VDSL2 and uses small pieces of spectrum next to VDSL2. Inspired by the Ericsson Radio Dot System, it challenges the femtocell paradigm offering full macro functionality in the small cells. An interesting service potential is offered albeit the added mobile traffic capacity is moderate as it is limited by the copper fronthaul. [1]

[1]Published in *Proc. IEEE International Conference on Communications (ICC 2015)*, London, United Kingdom, 08-12 Jun. 2015.

6.1 INTRODUCTION

The copper access network plays a key role in the evolutionary process of delivering broadband services [1]. Relaying radio signals over high-quality copper cables, as demonstrated by the system introduced in [2], can provide full macrocell functionality to indoor small cells fed over cables. While [2] focuses on indoor-enterprise environments using standard LAN cables, we pose the question whether it could be used to realize a vision of connected homes exploiting the edge of the access network. Given the increased interest in residential small cells in standardisation bodies and the increasing market uptake of femtocells, the concepts presented in [2] could be extended to the public switched telephone network (PSTN), representing a valuable market opportunity for operators.

The amount of attention given to residential small cells is increasing fast. This is partly fueled by increasing capacity demands calling for a densification of the cellular networks and insights into the cost of doing so [3]. Estimations in [4] [5] hint that between 70% and 90% of the traffic in the mobile networks is generated indoors, and it is suggested that the homes are natural new sites for small cells. But the drive towards small cells is also coming from changes in how we live and how we construct our dwellings. Thick fire-safe concrete walls increasingly block radio waves as we move our systems higher up in frequency. New window types with high energy insulation often have a built-in thin metal layer sealing off the interior both thermally and electromagnetically. Achieving indoor coverage becomes increasingly difficult without placing an antenna inside the home.

The main approach to get an antenna inside the home today is by deploying a femtocell. Here we go deeper into the Radio Dot System [2] idea presented by Ericsson. Instead of using standard LAN cables, we focus on twisted pairs in the PSTN copper plant, using the spectrum above VDSL2 17 MHz profiles but below G.fast (the next generation DSL) and maintaining so low interfering signal levels that these and other legacy systems remain unaffected at large. Thus, we argue that the extended concept is realistic and deployable, albeit it requires similar augmentation of the regulatory regimes like any new DSL system would. We perform the spectrum planning by optimizing for capacity in a typical plant topology and show that decent bit rates can be delivered. In [6] and [7], an alternative femtocell architecture is investigated. It superimposes the radio signal on the lower part of VDSL2 spectrum, starting from 100 kHz, and performs compound MIMO processing over air and cable channels. Although benefiting from lower cable attenuation, directly usage of VDSL2 spectrum makes this system suffer from inevitable VDSL2 interference, and vice versa.

In this paper we intend to develop a realistic and deployable system archi-

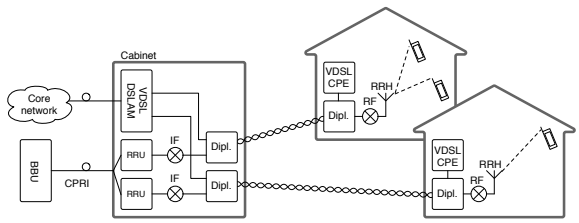

Figure 6.1: A schematic for the proposed radio-over-copper system. Notice the co-location of DSL equipment and remote radio units in the cabinet.

tecture that is collocated with VDSL2 in the cabinets of the telephony copper network. We extend the concept presented in [2] by evaluating its feasibility over regular telephony cables, using the spectra between VDSL2 [8] and G.fast [9]. Disregarding the losses in the radio channel, the available capacity in the copper loop is evaluated at the chosen band. We optimize the placement of downlink and uplink bands to avoid interfering with legacy systems, and as a result determine the maximum loop lengths over which radio signals can be deployed.

The paper is organized as follows. In Section 6.2, the system concept is introduced. In Section 6.3, achievable throughput and coexistence are investigated. Section 6.4 presents a case study with gap-band optimization and Section 6.5 concludes the work.

6.2 WHY AND WHERE

The system topology considered in this paper is depicted in Fig. 6.1. We have a location such as a home connected with telephony wiring feeding radio equipment in turn accessing an indoor radio channel. A traditional femtocell architecture terminates the copper line with some flavor of DSL, say VDSL2, backhauling the femtocell traffic over a bitstream connection. Suppose that we now want to deliver an analog fronthaul service over the copper but in parallel to VDSL2 rather than using it as backhaul. Is it possible and if so what capacity do we release? These are the questions we attempt to answer with this paper.

In Fig. 6.1 the base band unit (BBU) is located centralised in the network, and the radio signal is sent out to the remote radio unit (RRU) digitally with *e.g.*, CPRI [10] using a fiber connection. The RRU in this setup is typically co-located with the VDSL2 digital subscriber line access multiplexer (DSLAM) in the cabinet. In the downlink direction, the radio signal is upconverted to

the band above the VDSL2 signal. A diplexer (Dipl. in the figure) combines the VDSL2 signal and the radio signal on the twisted pair. At the customer premises a second diplexer splits the signals for the VDSL2 customer premises equipment (CPE) and the remote radio head (RRH). Shifting the radio signal up in frequency to the required band gives indoor mobile coverage. A similar procedure occurs in the uplink direction, where the RRH down-converts the radio signal to adequate frequencies in the copper loop. After transmission through the twisted pair, the analog radio signal is sampled at the RRU.

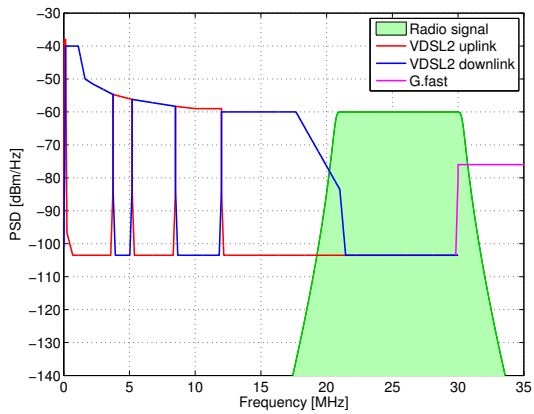

Figure 6.2: Bandplans for VDSL2, G.fast and the band of interest for the proposed radio-over-copper system, pictured as a green shaded area.

The frequency range we intend to make use of is shown in Fig. 6.2. The leftmost part of the figure shows the various up- and downlink bands of VDSL2 and the right part shows one of the possible options for the starting frequency of G.fast (30 MHz). This particular spectrum plan was defined by ITU [11] and is typical for what can be expected in many countries. Although VDSL2 30 MHz profiles have been standardized for years, their market penetration in western countries is much lower compared to their 17 MHz counterparts. Therefore, in this paper we target unused spectra between 17 MHz and 30 MHz.

The focus of this work is on spectrum planning and throughput evaluation. Several related issues are left for further study. First, we do not consider crosstalk originating from VDSL2 or G.fast users in neighboring lines. The band we intend to use lies spectrally between VDSL2 and G.fast. Thus, there is only crosstalk of leakage signals at the band edges. Second, we assume that there is no crosstalk in the VDSL2-G.fast gap band from other radio-over-copper systems—that is, we limit our focus to scenarios with a single

radio-over-copper system in the last-drop cable. This assumption is reasonable because the crosstalk between radio-over-copper systems could be dealt with by crosstalk cancellation schemes similar to those used in VDSL2 and G.fast. Third, we do not consider the impact of electromagnetic compatibility. In order to limit unwanted radio egress, we keep the transmit PSD in the band of interest between $-60\,\mathrm{dBm/Hz}$ and $-80\,\mathrm{dBm/Hz}$. This choice of transmit PSD is compatible with the limiting PSD masks defined for 30 MHz VDSL2 profiles. Consequently, the egress noise generated by the proposed system would be comparable to that caused by a standard-compliant 30 MHz VDSL2 system. However, analog radio-over-copper transmission remains vulnerable to radio ingress. Interference that is picked up by the copper pair in the gap band directly affects the signal quality, both in downlink and uplink direction. The coexistence analysis presented in the following sections is merely a first step in assessing the feasibility of an analog radio-over-copper system hosting a radio signal between VDSL2 and G.fast.

6.3 COEXISTENCE AND CAPACITY

In our system analysis, we begin by placing the downlink band for the radio signal starting at 21 MHz. Assume the VDSL2 system uses a bandplan occupying frequencies up to 17 MHz (*e.g.*, the FDD bandplan 998ADE17 [8]). Appropriate signal separation through the diplexers pushes the out-of-band leakage from VDSL2 right to the noise floor of the radio signal, and vice versa. The VDSL2 bandplan 998ADE17 shown in Fig. 6.2 ends with a downlink band in 12-17 MHz. The diplexer filters separating the signals will work on similar power levels, since both are either attenuated (on the RRH side) or un-attenuated (on the RRU side). The alternative to start with the uplink for the radio signal results in an unbalance of amplitudes, which requires substantially more attenuation in the stop band of the filters.

The narrowest bandwidths used in a modern mobile communication system, such as LTE [12], are 1.4 MHz, 3 MHz and 5 MHz, each having a built-in guard band. Unfortunately, two of the 5 MHz bands do not fit into our intended spectrum span from 21 MHz to 30 MHz and two 1.4 MHz bands yield a perhaps less than impressive capacity. Thus we focus on fitting two of the 3 MHz bands. This gives a single parameter to be optimized for the resulting capacity, namely the starting frequency of the 3 MHz uplink band.

6.3.1 DOWNLINK

Fig. 6.3 depicts a schematic band plan. The downlink signal is notably attenuated after transmission over the copper cable (cf. blue spectrum in Fig. 6.3a). The sloped shape of the in-band downlink spectrum is due to the low-pass

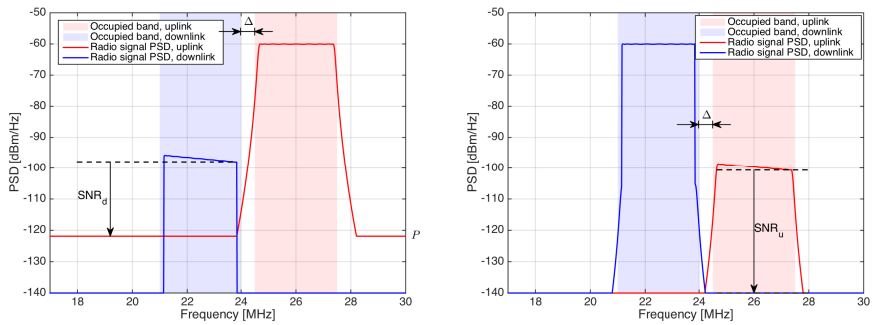

(a) RRH side **(b)** RRU side

Figure 6.3: Mutual interference between uplink and downlink radio signals in the copper cable.

properties of the cable where the attenuation grows with frequency. This sloped shape will be corrected by an equalizer at the RRH, since the PSD of the transmit signal at the antenna should be flat. At the RRH side of the copper line, the uplink signal is un-attenuated and thus much stronger than the downlink signal. The spectrum (red in Fig. 6.3a) is stronger and flat over the utilized band. However, the out-of-band leakage, *e.g.*, resulting from the insufficiently suppressed air channel interference, into the downlink signal can be severe if the guard band is not sufficient. After equalization of the downlink signal, the uplink spectrum (red) leaking into the downlink region (blue) will act as in-band interference, which is much stronger than the cable noise.

Let SNR_d denote the downlink SNR defined as the minimum ratio between the downlink signal PSD level and the out-of-band leakage PSD level P from the uplink signal. The level P encountered in a system depends strongly on implementation details. In a real system, P will rather vary over frequency than remain constant over our band of interest. However, from an analysis-perspective, a frequency-flat upper-bound leakage level P is sufficient since higher SNR levels over parts of the downlink band cannot be exploited by our analog relay scheme. In general, a larger gap-band Δ between downlink and uplink yields a lower interference level P and thus higher SNR_d, since the out-of-band leakage of uplink is supposed to be fading out. From an optimization perspective, it is thus rewarding to push the starting frequency of the uplink band upwards in frequency.

We start evaluating the proposed scheme by calculating the peak bit rate supported by the downlink radio link with a single antenna. We then calculate the SNR_d after transmission over the copper loop, while varying the loop

length and assuming different levels of leakage between uplink and downlink signals. The objective is to find the reach over which the system could be deployed, given some implementation losses due to band placement. We utilize the BT-CAD55 [13] cable model, since it is representative for copper cables deployed in the field.

Assuming an allowed symbol error rate[2] of 10^{-6} the SNR gap becomes $\Gamma \approx 9$ dB [14]. Then the bit rate supported by the copper channel in either direction can be obtained by

$$R_b = B(1-\beta)\log_2\left(1+10^{(\mathrm{SNR}-\Gamma)/10}\right) \tag{6.1}$$

where B denotes the transmission bandwidth and β is the fraction of B reserved for the built-in guard-bands, yielding the effective bandwidth $W = B(1-\beta)$. A radio signal with 3 MHz bandwidth and $\overline{R}_b^{[d]} = 11$ Mbps downlink peak bit rate is used as a reference.

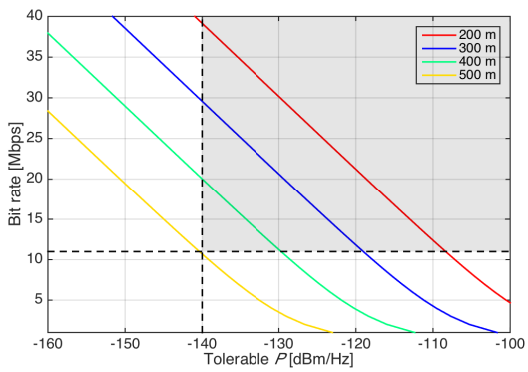

Figure 6.4: Bit rate supported by the copper channel for downlink radio signal over the BT-CAD55 cable model, assuming a certain interference from uplink leakage.

To enable radio transmission without performance degradation, R_b, the bit rate supported by the copper channel should not be lower than $\overline{R}_b^{[d]}$. Fig. 6.4 presents the relation between R_b at the far-end of the copper pair and the uplink leakage PSD level P. Given different loop lengths, the insertion loss for the copper cable BT-CAD55 was calculated as in [13]. The background noise on the copper pair limits the noise-plus-interference level inside the downlink band to -140 dBm/Hz. Thus, the grey area in Fig. 6.4 represents the feasible region for downlink radio transmission over the BT-CAD55 test-loop.

[2]Note that the symbol error rate is an upper bound for the bit error rate.

6.3.2 UPLINK

At the RRU side of the copper cable the situation is mirrored as the uplink band is attenuated and the downlink out-of-band leakage causes interference (see Fig. 6.3b). The achievable rate R_b in uplink direction versus downlink leakage PSD is very similar to the results presented in Fig. 6.4. However, there is one more effect. The uplink signal will be more attenuated the further up in frequency it is placed. Furthermore, the interference to and from G.fast services increases as the upper edge of the uplink band moves towards 30 MHz. From an optimization perspective, there exists a trade-off between increased attenuation and larger gap-band.

Clearly, we would like to stay away from the future G.fast band starting at 30 MHz for the sake of both services, but we do not include any specific level of interference in the derivation at this point. The G.fast out-of-band noise decreases very sharply and would not have an impact on the results at least in this direction.

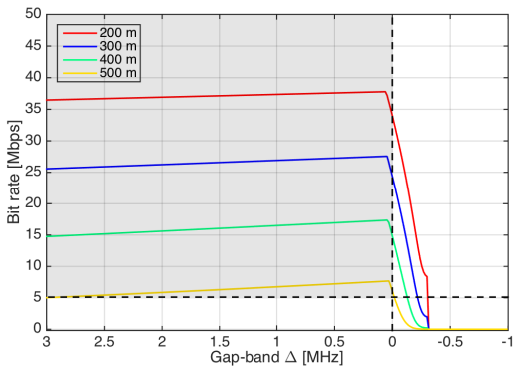

Figure 6.5: Bit rates supported by the copper channel for uplink radio signal over the BT-CAD55 model, assuming a certain gap-band Δ.

Let Δ denote the gap-band between uplink and downlink. Assume that at the near-end of the copper cable, the baseband downlink radio signal is shifted to the adequate copper frequencies, but does not go through any power amplifier, resulting in a sharply declining PSD at the band edges. The well behaved downlink radio signal results in negligible out-of-band emissions. Typically, the maximum uplink bit rate is $\overline{R}_b^{[u]} = 5\,\text{Mbps}$. Using this value as a reference and varying Δ, we obtain the uplink feasible region shown in Fig. 6.5. Combining the feasible regions in both directions, we observe that the system could be deployed almost 500 meters away from the cabinet for

the BT-CAD55 cable.

6.4 BAND PLACEMENT WITH FIXED FILTER STRUCTURE

In this section we evaluate the impact of band placement given a certain fixed diplexer structure. For this case study, we use the spectra shown in Fig. 6.3. Applying the same methodology as before, we vary Δ, cable length, transmit PSD, and cable type while using the peak radio signalling bit rates as a lower-bound threshold for feasibility.

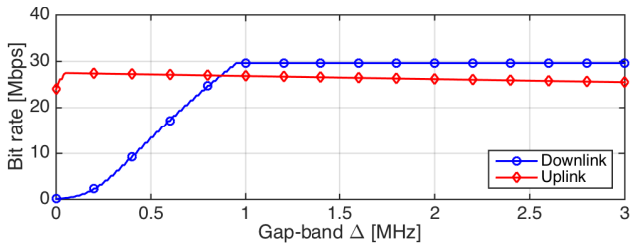

(a) Bit rates in both directions over 300 m copper pair.

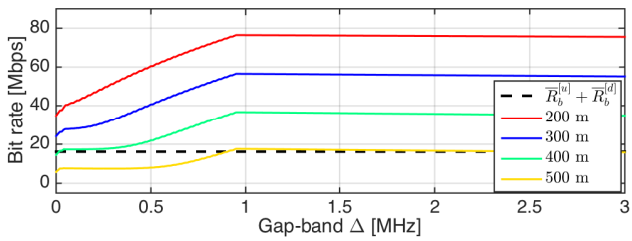

(b) Aggregate bit rates.

Figure 6.6: Supported bit rates for the radio signal over BT-CAD55 copper pair, when the transmit PSD is -60 dBm/Hz.

In Fig. 6.6a the available bit rates over the copper channel for downlink and uplink directions are shown as a function of the gap-band Δ. We chose a 300 meters BT-CAD55 copper pair to obtain a representative attenuation level. The downlink band is positioned at 21-24 MHz, while the uplink band moves depending on Δ. For small Δ, the interference between the two bands can be substantial. As Δ grows, mutual interference fades and there is a frequency point where the downlink band is not interfered anymore, or the interference power level becomes lower than the background noise on the twisted pair. Beyond this frequency point, the bit rate remains constant, *e.g.*, in Fig. 6.6a typically after $\Delta = 0.95$ MHz. For the uplink band, signal attenuation

increases for larger values of Δ, consequently causing a decrease in bit rates.

The aggregate bit rates are presented in Fig. 6.6b, assuming a transmit PSD of $-60\,\mathrm{dBm/Hz}$ in both directions. As expected, the aggregate bit rate peaks for $\Delta = 0.95\,\mathrm{MHz}$. At this point, mutual interference reaches the background noise level, and the uplink band is located as close to downlink as possible. At the optimal gap-band setting, the upper edge of uplink stops before 28 MHz, leaving a comfortable gap between the proposed system and future G.fast services.

The maximum transmit power also affects optimal gap-band setting, as evidenced in Fig.6.7a. For a fixed filter structure with a particular side-lobe suppression capability, higher in-band transmit power implies increased out-of-band leakage. Therefore, a wider gap-band is required. Lower transmit power allows for shorter gap-bands, but the drop in receive SNR might not justify that choice (see Fig.6.7b). High transmit-power levels, however, may cause undesirable leakage into neighboring systems on the same copper pair as well as crosstalk.

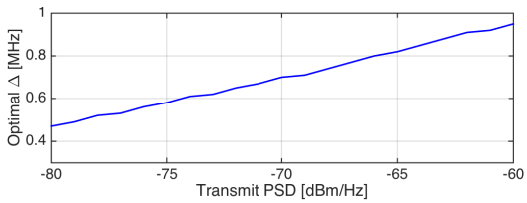

(a) Relation between transmit PSD and optimal Δ.

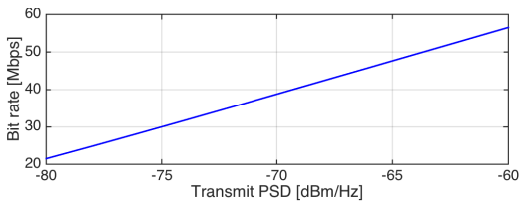

(b) Aggregate bit rates when the optimal Δ is applied.

Figure 6.7: Influence of allowed transmit PSD on the band placement, assuming a fixed filter structure in the RRH.

The cable channel will not severely affect the total SNR of the combined copper and air channel as long as the available bit rate for the copper segment is well above the peak rate for the air interface. Using this reasoning we evaluate possible deployment distances. In this study case, besides BT-CAD55, we employ two other cables models, ETSI90 and ETSI32, representing high and low quality cables, respectively. The results are collected in Fig. 6.8,

where the aggregate bit rate is shown as a function of cable length, assuming $\Delta = 0.95\,\text{MHz}$, a transmit PSD of $-60\,\text{dBm/Hz}$, and the same fixed filter structure for all cables.

For the BT-CAD55 cable, a length close to 500 meters approaches the air interface peak rate. For the low quality cable the same limit is at about 360 meters while the high quality cable has a substantial margin even at 500 meters. We conclude that it is possible to transmit analog radio signals for modern communication systems over the telephony copper lines connecting the end user in ranges of at least 350 meters. For medium quality cables this measure is close to 500 meters and for high quality well above 500 meters.

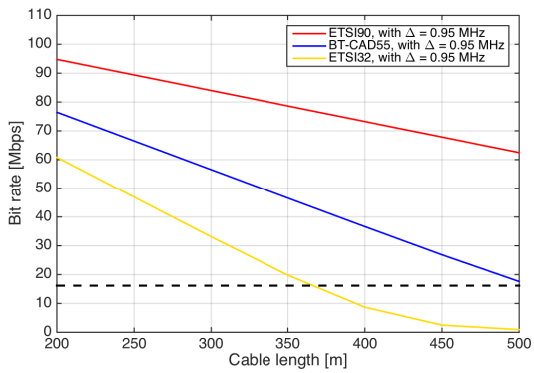

Figure 6.8: Achievable aggregate bit rates over the copper channel using the optimal gap-band setting, when the transmit PSD is $-60\,\text{dBm/Hz}$.

6.5 CONCLUSION

Small cells seem to be the next solution to the ever growing capacity demand in mobile networks, which is fueled by the development of more and more sophisticated services and mobile terminals as well as a growing number of users. Relaying the radio signal over the existing copper access network may provide a valuable contribution to solving both the backhaul bottleneck and placing small cells right where they are needed. We argue that a cabinet-based system is realistic in terms of coexistence with wireline systems and we show that the capacity it delivers is significant. The added capacity is sufficient to deliver decent mobile services to most homes given a typical European topology of the PSTN network. Peak capacity is limited by the copper fronthaul bandwidth but average capacity per user is good as these residential small cell naturally has few users.

References

[1] P. Ödling, T. Magesacher, S. Höst, P. Börjesson, M. Berg, and E. Areizaga, "The fourth generation broadband concept," *IEEE Communications Magazine*, vol. 47, no. 1, pp. 62–69, January 2009.

[2] C. Lu, M. Berg, E. Trojer, P.-E. Eriksson, K. Laraqui, O. V. Tidblad, and H. Almeida, "Connecting the dots: small cells shape up for high-performance indoor radio," *Ericsson Review*, vol. 91, December 2014. [Online]. Available: http://goo.gl/YvdY5N

[3] Ericsson AB, "Ericsson mobility report: On the pulse of the networked society," whitepaper, 2014. [Online]. Available: http://goo.gl/QjdGbn

[4] Mobidia, "Understanding the role of managed public Wi-Fi in todayâĂŹs smartphone user experience: A global analysis of smartphone usage trends across cellular and private and public Wi-Fi networks," whitepaper, 2013. [Online]. Available: http://goo.gl/rCOfR4

[5] Cisco, "The zettabyte era: Trends and analysis," whitepaper, 2014. [Online]. Available: http://goo.gl/p7KX4a

[6] J. Gambini and U. Spagnolini, "Radio over telephone lines in femtocell systems," in *Proc. 2010 IEEE 21st International Symposium on Personal Indoor and Mobile Radio Communications (PIMRC)*, September 2010, pp. 1544–1549.

[7] ——, "Wireless over cable for femtocell systems," *IEEE Communications Magazine*, vol. 51, no. 5, pp. 178–185, May 2013.

[8] ITU, "Very high speed digital subscriber line transceivers 2 (VDSL2)," Recommendation ITU-T G.993.2, December 2011. [Online]. Available: http://www.itu.int/rec/T-REC-G.993.2/en

[9] ——, “Fast access to subscriber terminals - physical layer specification,” Recommendation Draft ITU-T G.9701, 2013. [Online]. Available: https://www.itu.int/rec/T-REC-G.9701/en

[10] Ericsson AB, Huawei Technologies, NEC Corporation, NSN and Alcatel-Lucent, “Common public radio interface specification v6.0,” Publicly available specification, 2013. [Online]. Available: http://www.cpri.info/spec.html

[11] ITU, “Fast access to subscriber terminals (FAST) âĂŞ Power spectral density specification,” Recommendation Draft ITU-T G.9700, April 2014. [Online]. Available: https://www.itu.int/rec/T-REC-G.9700/en

[12] 3GPP, “LTE; Evolved universal terrestrial radio access (E-UTRA); Base station (BS) radio transmission and reception,” Tech. Rep., 2011.

[13] D. Acatauassu, S. Höst, C. Lu, M. Berg, A. Klautau, and P. O. Börjesson, “Simple and causal copper cable model suitable for g.fast frequencies,” *IEEE Transactions on Communications*, vol. 62, no. 11, pp. 4040–4051, November 2014.

[14] J. G. Proakis, *Digital Communications*, 4th ed. Mc Graw Hill, ISBN 0-07-232111-3, 2001.

7

LTE Over Copper - Potential and Limitations

Yezi Huang, Eduardo Medeiros, Nilma Fonseca, Stefan Höst,
Thomas Magesacher, Per-Erik Eriksson, Chenguang Lu,
Per Ödling and Per Ola Börjesson

Abstract

The densification of mobile networks in order to meet increased capacity demands is ongoing, needed and costly. A few papers have been published based on the insight that the fixed broadband networks offer a multitude of sites, for instance our homes, for potential small cell deployment providing backhaul capacity and power without site costs. However, in order to reach economical large-scale benefits, we explore the case when radio systems are deployed in coexistence with DSL. In this paper, we establish the feasibility of such a concept under constraints invoked by state-of-the-art and emerging systems (3GPP, VDSL2 and G.fast) and make statements about the required architecture. We also point out that the enthusiasm of previously published results should be lowered a notch. [1]

[1]Published in *Proc. IEEE Symposium on Personal, Indoor and Mobile Radio Communications - (PIMRC)*, Hong Kong, China, 30 Aug. - 03 Sep. 2015.

7.1 INTRODUCTION

The explosive growth of connected smart devices forces operators to invest constantly in improving the capacity of mobile radio networks. Currently, the main approach for addressing the demands is to deploy closely spaced macro base stations. With 4G deployments reaching maturity and the telecom industry starting their research on candidate solutions for 5G, small cells are promoted as an important enabler for higher capacity.

In the papers [1] [2] Gambini *et al.* proposed the reuse of copper lines for the deployment of femtocells based on amplify-and-forward devices. In [3], Lu *et al.* present a solution for increased indoor radio performance. Their system benefits from transparent remote radio heads (RRHs) and shared baseband processors to achieve full coordination between small cells and the macro layer, eliminating the main drawback of femtocells.

In [4] we have evaluated the feasibility of co-deploying fronthaul for modern radio access network together with traditional digital subscriber line (DSL) services, reusing the cabinet infrastructure already in place. Our results suggest that mobile networks with moderate capacity could be deployed over copper without disturbing legacy fixed-access technologies.

In this paper we utilize the basic architecture described in [4] to deploy LTE for small cells over residential unshielded copper loops. Our interest is to investigate the implications of 3GPP compliance on an implementation that down/up converts LTE signals to intermediate frequency (IF) over the copper loops, as illustrated in Fig. 7.1. Based on the requirements we present design guidelines for an RRH and estimates for how distant these systems could be deployed from the street cabinet.

7.2 SYSTEM ARCHITECTURE

We consider a distributed base station architecture as described in [4] where the cell processing is functionally split among three entities. Baseband processors perform digital signal processing on baseband LTE signals. In downlink direction the baseband signals are up-converted to IF (labeled in Fig. 7.1) at a remote radio unit (RRU) deployed in colocation with DSL equipment in street cabinets. After IF conversion, the LTE signals are transmitted over a copper pair (represented in Fig. 7.1) to an RRH, converted to the appropriate radio frequency (RF) and then sent to the user equipment (UE) over the air. In the uplink direction, the radio signal received at the RRH is down-converted to IF, transmitted to the RRU, and finally converted to baseband for receiver processing.

To coexist with VDSL2 and G.fast systems, the target IF band is placed between 21 MHz and 30 MHz, which restricts the available bandwidth for

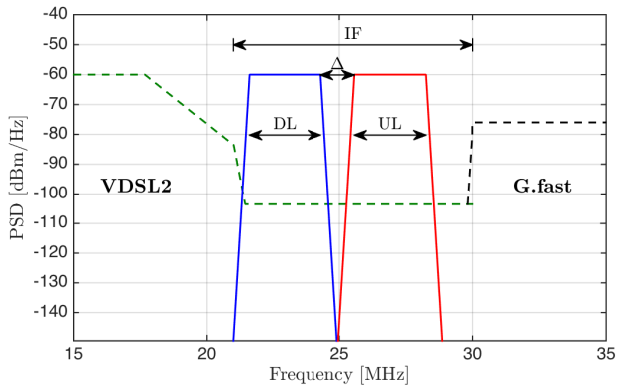

Figure 7.1: Bandplan adopted in this paper. The LTE signal is placed between VDSL2 and G.fast systems for coexistence. The dashed lines represent the limit PSD masks for the DSL systems. The frequencies between 17 MHz and 30 MHz are not used by VDSL2 17 MHz profiles or G.fast.

LTE signals to be 3 MHz. The resulting bandplan is presented in Fig. 7.1, with the downlink LTE band placed between 21 MHz and 24 MHz, a gap-band of $\Delta = 0.95$ MHz, and the uplink signal extending to 28 MHz. As reported in [4], for a maximum transmit PSD of $S = -60$ dBm/Hz over the copper pair, the proposed system can be deployed up to 500 meters away from street cabinets.

In Fig. 7.2 we present a model for the RRH considered in this work. The upper and the lower signal branches, which contain the processing elements for the LTE downlink (DL) and the LTE uplink (UL) path, are connected to the twisted pair via a hybrid coupler. On the opposite side they connect to an RF front-end. The hybrid coupler used in the RRH is not perfect, exhibiting non-negligible trans-hybrid loss [5], denoted as L_{hybrid}. The leakage from uplink to downlink inside the RRH may cause in-band interference and/or out-of-band noise that need to be dealt with in order to avoid performance degradation.

Invoking the requirements imposed by 3GPP regulations and a typical indoor propagation scenario, feasible quantities for the overall in-band amplification G and out-of-band rejection L at the RRH can be derived for uplink and downlink, respectively. Here we perform a "black-box" study without suggesting a specific arrangement of amplifiers and filters. Superscripts [u] and [d] are used to distinguish between uplink and downlink, respectively.

The choice of in-band gains depends on the required transmit power over copper and air channels such that the necessary SNR is achieved. In order to avoid mutual interference and also coexist with other wireless systems that

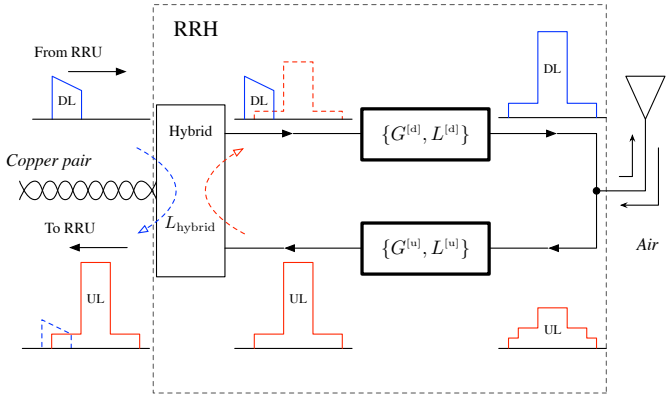

Figure 7.2: Model for the RRH. For each direction in-band gain and out-of-band rejection are the parameters. Leakage from uplink to downlink due to an imperfect hybrid is represented by the red dashed arrow.

operate on adjacent channels, out-of-band rejections are derived according to spectrum emission mask (SEM) and adjacent channel selectivity (ACS) in uplink direction and required adjacent channel leakage power ratio (ACLR) in downlink direction, respectively.

7.3 UPLINK PATH

7.3.1 IN-BAND SIGNAL AMPLIFICATION $G^{[U]}$

For the uplink direction, we start by estimating the receive power at the RRH antenna. Here we employ the indoor transmission path-loss model [6], which assumes that base station and UE are located in the same building. We calculate the air channel path-loss for a typical residential scenario as

$$L_{\text{air}}\,[\text{dB}] = 20\log_{10} f_c + \alpha \log_{10} r + L_f - 28, \tag{7.1}$$

for a carrier frequency f_c [MHz], a propagation distance r [m] and an indoor environment characterized by distance power loss coefficient α and floor penetration loss factor L_f [dB]. The path-loss L_{air} increases with the distance r between RRH antenna and UE.

For a 3 MHz LTE signal, the uplink peak bit-rate is $\widetilde{R}_{\text{u}} = 7.5$ Mbps. The receive SNR at the RRU required to support the peak rate after copper transmission is

$$\widetilde{\text{SNR}}^{[\text{u}]}\,[\text{dB}] = 10\log_{10}\left(2^{(\widetilde{R}_{\text{u}}/B_{\text{c}})-1}\right) + \Gamma, \tag{7.2}$$

where $B_c = 2.7\,\text{MHz}$ is the transmission bandwidth configuration [7] and $\Gamma = 9\,\text{dB}$ is reserved to cover implementation losses. Since the maximum output power of the UE is 23 dBm [8], the maximum receive power at the RRH antenna connector is given by $P^{[u]}_{\text{rx,ant}}\,[\text{dBm}] = 23 - L_{\text{air}}$. Considering thermal noise as the only noise source for the air channel transmission, we can derive the receive SNR at the RRH antenna connector for a certain L_{air}, denoted $\text{SNR}^{[u]}_{\text{air}}$. In this work, we assume that the uplink noise figure in the RRH is 0 dB. The uplink SNR before copper transmission then stays the same as $\text{SNR}^{[u]}_{\text{air}}$. To deliver $\widetilde{\text{SNR}}^{[u]}$ to the RRU, the related SNR required for copper transmission is calculated in linear scale as

$$\text{SNR}^{[u]}_{\text{Cu}} = \frac{\text{SNR}^{[u]}_{\text{air}} \cdot \widetilde{\text{SNR}}^{[u]}}{\text{SNR}^{[u]}_{\text{air}} - \widetilde{\text{SNR}}^{[u]}}. \tag{7.3}$$

For a given cable type, the channel attenuation L_{Cu} is a monotonically increasing function with respect to both frequency f and cable length d. Let $\mathcal{F}^{[u]}$ denote the IFs occupied by each uplink LTE subcarrier as shown in Fig. 7.1. To derive the in-band SNR, we use the sub-carrier that experiences the worst case attenuation as a reference. Given the cable noise PSD of $N = -150\,\text{dBm/Hz}$ and using Eq. (7.3) in dB-scale, the uplink transmit power over the copper should be

$$P^{[u]}_{\text{tx,Cu}}\,[\text{dBm}] \geq \text{SNR}^{[u]}_{\text{Cu}} + (N + 10\log_{10}B) + \max_{f \in \mathcal{F}^{[u]}} L_{\text{Cu}}(f, d). \tag{7.4}$$

Assuming a maximum transmit PSD over the copper as $S_{\max} = -60\,\text{dBm/Hz}$, one can also estimate the preliminary maximum distance over which such RRH could be deployed from the cabinet for $(P^{[u]}_{\text{tx,Cu}} - \log_{10}B) \leq S_{\max}$.

The necessary amplification in uplink direction can then be calculated as

$$G^{[u]}\,[\text{dB}] = P^{[u]}_{\text{tx,Cu}} - P^{[u]}_{\text{rx,ant}}. \tag{7.5}$$

Equivalently, the maximum deployable cable length d fulfilling Eq. (7.4) can be estimated given a certain available $G^{[u]}$.

In Fig. 7.3 we present the relationship between maximum cable length d (distance between cabinet and RRH deployment site) and the maximum path-loss that the system can endure while still providing the LTE uplink peak bit-rate. For our target deployment scenario, an indoor residential environment at 1.8 GHz, typical values for α and L_f in Eq. (7.1) are 28 and 10 dB respectively. Notice that to deploy long cables there will be a decrease in the maximum acceptable path-loss corresponding to the gaps between solid lines and the red dashed line in Fig. 7.3. We refer to this gap as ΔL_{air}. The ΔL_{air} varies

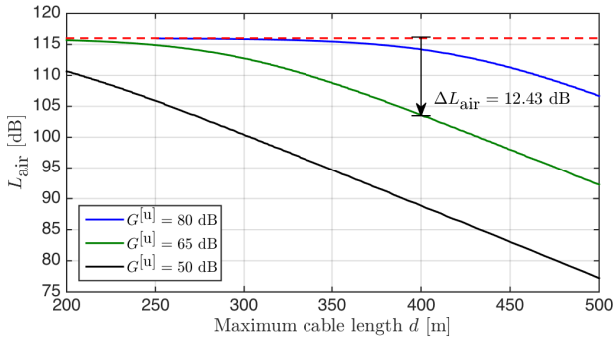

Figure 7.3: The three solid curves represent the relationship between deployment distance and the tolerable path-loss in the air for a fixed $G^{[u]}$. The red dashed line represents the initial maximum acceptable path-loss for the LTE uplink peak bit-rate. The ΔL_{air} increases with cable length as exemplified by the arrow around 400 meters.

for the same deployed cable length with different $G^{[u]}$ available. The cable attenuation used to obtain these curves is calculated using the BT-CAD55 model, commonly employed to estimate capacity in DSL system design [9].

7.3.2 OUT-OF-BAND REJECTION $L^{[U]}$

As sketched in the signal flow depicted in Fig. 7.2, after air channel transmission, the received signal at the RRH may contain, besides the signal of interest, out-of-band compontents $\text{OOB}_{\text{ant}}^{[u]}$ at the antenna connector. Passing through the amplifying element(s) at the RRH, those out-of-band components experience the same gain as the in-band uplink signal. Although this causes no trouble for the uplink transmission in itself, the out-of-band noise may lower the quality of the downlink signal due to the hybrid leakage. With less than 3 MHz gap-band between downlink and uplink in the copper channel, any neighboring interference captured by the RRH antenna will leak via the hybrid coupler and overlap with the signal in the downlink processing path.

To guarantee the quality of the in-band signal transmission in downlink direction, the error vector magnitude (EVM) of transmitted signals should be lower than the limits listed in Table 6.5.2-1 in [7]. EVM is defined as

$$\text{EVM} = \sqrt{\frac{1}{K}\frac{\|\mathbf{y}-\mathbf{x}\|_2^2}{P_0}} \cdot 100\%,$$

where $\mathbf{x}$ and $\mathbf{y}$ denote the constellation symbols at the RRU and RRH antenna connector respectively, K is the number of involved symbols, and P_0

is the average power of the modulation scheme used. This quantity can also be translated to an in-band SNR requirement in the downlink direction given by $\widetilde{\mathrm{SNR}}^{[\mathrm{d}]} \approx 1/\mathrm{EVM}^2$. Accordingly, the minimum $\widetilde{\mathrm{SNR}}^{[\mathrm{d}]}$ is around 15.14 dB for QPSK, 18.06 dB for 16-QAM, and 21.98 dB for 64-QAM. These parameters suggest that a general minimum value of $\widetilde{\mathrm{SNR}}^{[\mathrm{d}]} = 21.98\,\mathrm{dB}$ should be guaranteed.

Since it is difficult to mitigate the resulting in-band interference in the downlink path, we should suppress out-of-band emission already in the uplink processing to a level such that the downlink EVM requirement is not violated. Considering the trans-hybrid attenuation L_{hybrid}, the permissible uplink out-of-band emission at the copper connecting port is

$$\mathrm{OOB}_{\mathrm{Cu}}^{[\mathrm{u}]}\,[\mathrm{dBm}] = P_{\mathrm{rx,Cu}}^{[\mathrm{d}]} - \widetilde{\mathrm{SNR}}^{[\mathrm{d}]} + L_{\mathrm{hybrid}}. \tag{7.6}$$

Here $P_{\mathrm{rx,Cu}}^{[\mathrm{d}]}$ is the signal power reaching the RRH after transmission over the copper channel, *i.e.*,

$$P_{\mathrm{rx,Cu}}^{[\mathrm{d}]}\,[\mathrm{dBm}] = S - \max_{f \in \mathcal{F}^{[\mathrm{d}]}} L_{\mathrm{Cu}}(f) + \log_{10} B. \tag{7.7}$$

Eq. (7.6) implies a rejection requirement at the RRH given by

$$L^{[\mathrm{u}]}\,[\mathrm{dB}] = P_{\mathrm{tx,Cu}}^{[\mathrm{u}]} - \widetilde{\mathrm{SINR}}^{[\mathrm{u}]} - \mathrm{OOB}_{\mathrm{Cu}}^{[\mathrm{u}]}, \tag{7.8}$$

where $\widetilde{\mathrm{SINR}}^{[\mathrm{u}]}$ is the power ratio between the uplink in-band signal and the maximum out-of-band component that overlaps with the downlink in-band signal.

To properly illustrate the influence of specific 3GPP requirements for the uplink out-of-band rejection we differentiate between two situations:

RRH WITHOUT AN ALIEN SYSTEM NEARBY

3GPP imposes SEM and spurious emission limits for the UE transmitter [8], which restrict the out-of-band spectral emissions. Assuming that a UE transmits at the worst case PSD mask according to those requirements, the signal received at the RRH after amplification is represented by the red solid curve in Fig. 7.4. If no filtering is performed, the uplink signal of interest plus its out-of-band components leak via the hybrid resulting in in-band interference to the downlink signal. Since the gap-band reserved between uplink and downlink over copper transmission is small, the leakage imposes a requirement on $L^{[\mathrm{u}]}$ as indicated by the arrow in Fig. 7.4.

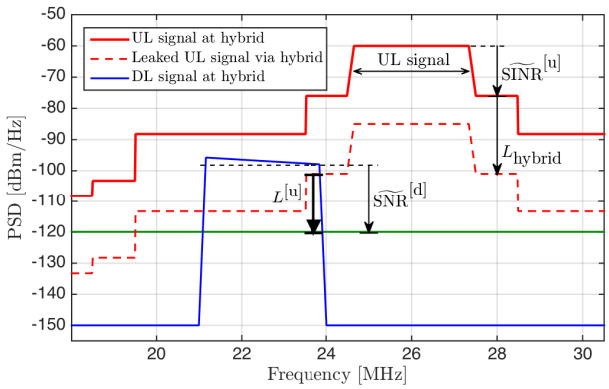

Figure 7.4: Leakage of uplink out-of-band emissions into the downlink signal. The red solid curve represents the received uplink signal after amplification at the RRH. The dashed curve represents the leakage PSD if no filtering is performed. The green solid curve represents the acceptable noise floor for downlink peak bit-rates. Calculated for 300 meters of BT-CAD55.

RRH WITH AN ALIEN SYSTEM NEARBY

3GPP also defines an ACS [7] metric in the uplink to coexist with other systems that operate in adjacent channels. It forces the base station receiver to be able to cope with high levels of interference from neighboring channels, which are within the receiver's operating band. This happens for example when a nearby terminal transmits with very high power to reach a distant macro-cell outside the building (*i.e.*, from another operator). The requirement suggests that an interference with a mean power of $\widetilde{P}_{\text{intf}} = 28\,\text{dBm}$ should be supported. When the interference from a nearby system is received and amplified it may impact downlink transmission as depicted in Fig. 7.5.

In Fig. 7.6 we present the relationship between the required out-of-band rejection $L^{[u]}$ and cable length d, with and without alien interference in adjacent channels, for a certain acceptable ΔL_{air}, assuming a trans-hybrid loss of $L_{\text{hybrid}} = 25\,\text{dB}$ [10]. In Fig. 7.6a, we consider the situation when the highest out-of-band emission below the SEM happens to partially overlap with the downlink in-band signal. Fig. 7.6b estimates the required $L^{[u]}$ in presence of the worst alien interference that ACS suggests.

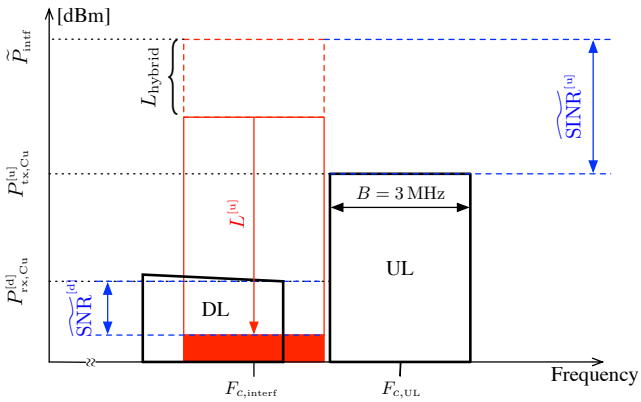

Figure 7.5: ACS requirement implications. A neighboring uplink transmission, represented as tall red rectangle must be suppressed to the solid red box in order to avoid drowning the downlink band. The uplink interference is captured at the RRH antenna and may overwhelm the downlink signal via the hybrid if no filtering is performed.

7.4 DOWNLINK PATH

For the downlink branch, the EVM requirement described in Section 7.3.2 also limits the preliminary maximum deployment distance of the proposed system. Given a fixed transmit PSD from the RRU as $S = -60\,\text{dBm/Hz}$ and a background noise PSD of $-150\,\text{dBm/Hz}$, the received SNR at the RRH decreases when using longer cables. At the largest deployment distance, the cable should deliver $\widetilde{\text{SNR}}^{[d]} = 21.98\,\text{dB}$ to the RRH in the downlink direction.

For a home base station with a single antenna, 3GPP stipulates a maximum transmit power $\widetilde{P}^{[d]}_{\text{tx,ant}} = 20\,\text{dBm}$ [7], which requires an in-band signal amplification of

$$G^{[d]}\,[\text{dB}] = \widetilde{P}^{[d]}_{\text{tx,ant}} - P^{[d]}_{\text{rx,Cu}}, \tag{7.9}$$

where $P^{[d]}_{\text{rx,Cu}}$ is the received power in downlink after copper transmission as calculated in Eq.(7.7).

Also in [7], 3GPP establishes that base stations should suppress adjacent channel signal leakage before passing the signal to the antenna. This requirement, known as ACLR, asks for either an adjacent channel leakage power of $-50\,\text{dBm/MHz}$ or a 45 dB attenuation compared to the in-band signal power. The less stringent number of the two is considered the limit. For our proposed RRH, the ACLR requirement leads to a total leakage power limit over

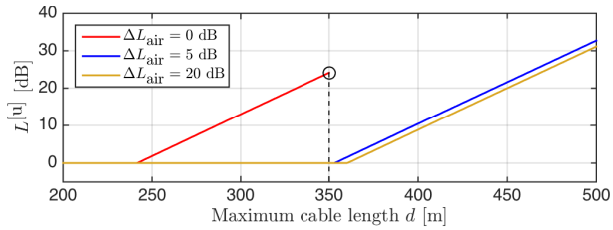

(a) Without alien system ($\widetilde{\mathrm{SINR}}^{[u]} = 16\,\mathrm{dB}$, $\widetilde{\mathrm{SNR}}^{[d]} = 21.98\,\mathrm{dB}$)

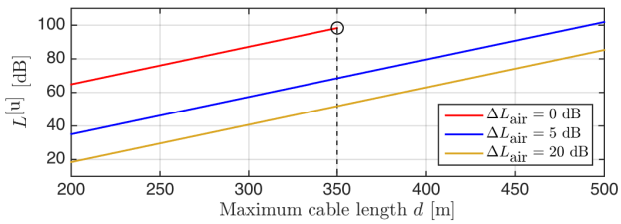

(b) With alien system ($\widetilde{P}_{\mathrm{intf}} = 28\,\mathrm{dBm}$, $\widetilde{\mathrm{SNR}}^{[d]} = 15.14\,\mathrm{dB}$)

Figure 7.6: Required uplink out-of-band rejection $L^{[u]}$ for different cable lengths. Each solid curve is calculated for an acceptable ΔL_{air}. The red curve is interrupted when the maximum transmit PSD is reached.

the neighboring channel of around $\widetilde{\mathrm{OOB}}^{[d]}_{\mathrm{ant}} = -25\,\mathrm{dBm}$.

If the uplink signal leaks into downlink transmission via the hybrid coupler, a big portion of the leakage can be transmitted to the antenna, disrupting neighboring bands. An example of this can be seen in Fig. 7.7, assuming the uplink out-of-band interference has been in good control. The effective leaked power from the uplink signal can be calculated as

$$\mathrm{OOB}^{[d]}_{\mathrm{Cu}}\,[\mathrm{dBm}] = P^{[u]}_{\mathrm{tx,Cu}} - L_{\mathrm{hybrid}},$$

To fulfil the ACLR requirement, the downlink out-of-band rejection must be

$$L^{[d]}\,[\mathrm{dB}] = \mathrm{OOB}^{[d]}_{\mathrm{Cu}} + G^{[d]} - \widetilde{\mathrm{OOB}}^{[d]}_{\mathrm{ant}}, \tag{7.10}$$

assuming that out-of-band interference at adjacent channels experiences the same amplification as the in-band signal.

As indicated in Eq. (7.7), the cable attenuation determines the amount of power received at the RRH. To obtain a flat transmit PSD at the antenna connector, each value of $P^{[d]}_{\mathrm{rx,Cu}}$ leads to a required $G^{[d]}$. This is illustrated in

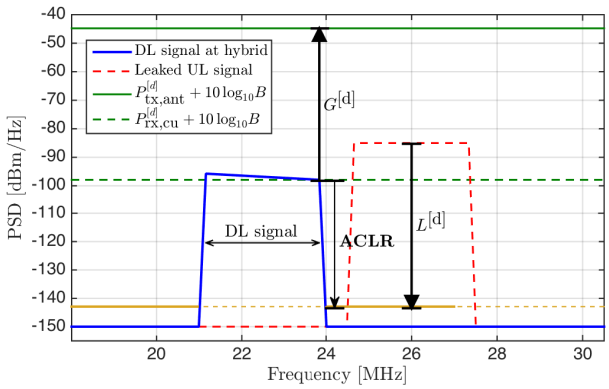

Figure 7.7: PSDs of 300 meters BT-CAD55 model in the downlink branch, after the hybrid coupler and before filtering. The signal of interest is the left lobe. The band to the right is the upstream signal coupled through the hybrid and should be suppressed to the ACLR level given in yellow.

Fig. 7.8a for different cable lengths. Also, the uplink signal is amplified before the hybrid, which in turn causes the increase of undesirable leakage through the hybrid. In order to fulfill the ACLR requirement, we must obey the downlink out-of-band rejection requirements depicted in Fig. 7.8b.

7.5 DESIGN IMPLICATIONS

By jointly considering the discussed 3GPP requirements and using the described methodology, one can obtain the desired values for total in-band gain and out-of-band rejection required at the RRH. As an example, we list three different designs in Table 7.1. The bold numbers in each row represent target values, which are prioritized and kept fixed.

For the first row, the acceptable ΔL_{air} is set to 0. This results in a deployment distance of around 350 meters, but very high $G^{[u]}$ and $L^{[u]}$. If alien systems are not a concern, the values in parenthesis should be considered for $L^{[u]}$. In the second row, we are aiming for a deployment distance of 400 meters with an acceptable ΔL_{air} of 5 dB. The requirements for $L^{[u]}$, $G^{[u]}$ and $L^{[d]}$ are relaxed due to the permissible ΔL_{air}, but the value for $G^{[d]}$ increases because of the increased cable length. In the last row, we start by fixing reasonable values for filtering and amplifying components, which limit the deployment reach to around 310 meters without increasing ΔL_{air} significantly.

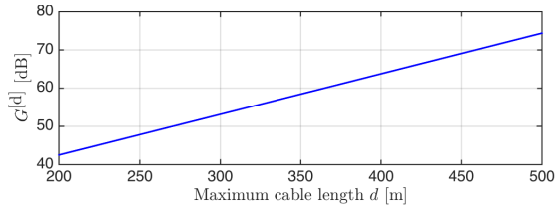

(a) On $G^{[d]}$

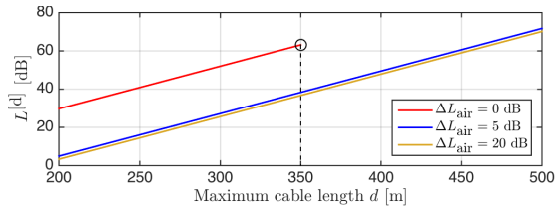

(b) On $L^{[d]}$

Figure 7.8: Influence of cable attenuation on RRH design parameters for downlink direction.

Table 7.1: Parameter values for different design objectives

ΔL_{air} [dB]	$L^{[u]}$ [dB]	$G^{[u]}$ [dB]	$L^{[d]}$ [dB]	$G^{[d]}$ [dB]	d [m]
0	98.30 (24.14)	80	63.16	58.45	350
5	79.62 (10.46)	74	49.48	63.76	**400**
5	**60**	**65**	**60**	**65**	310

7.6 CONCLUSION

Although our results in [4] suggest that modern OFDM-based radio systems could be deployed over copper up to 500 m, once 3GPP requirements are taken into consideration we observe absurdly stringent filtering and amplifying demands in Fig. 7.3, 7.6b and 7.8a, and also limited deployment distance if we do not compromise on radio reach. For as small a gap-band as assumed here, fulfilling 3GPP requirements practically prohibits fully analog implementations, such as the one presented in [1] and [4]. However, with digital filtering in the RRH and reasonable small cell assumptions, we conclude that LTE over copper lines is a technically viable concept. A myriad of small cells could be added to the mobile networks using the existing fixed infrastructure as a base without offending the technical foundations of currents standards and regulations.

References

[1] J. Gambini and U. Spagnolini, "Radio over telephone lines in femtocell systems," in *Proc. 2010 IEEE 21st International Symposium on Personal Indoor and Mobile Radio Communications (PIMRC)*, September 2010, pp. 1544–1549.

[2] ——, "Wireless over cable for femtocell systems," *IEEE Communications Magazine*, vol. 51, no. 5, pp. 178–185, May 2013.

[3] C. Lu, M. Berg, E. Trojer, P.-E. Eriksson, K. Laraqui, O. V. Tidblad, and H. Almeida, "Connecting the dots: small cells shape up for high-performance indoor radio," *Ericsson Review*, vol. 91, December 2014. [Online]. Available: http://goo.gl/YvdY5N

[4] Y. Huang, E. Medeiros, S. Höst, T. Magesacher, P.-E. Eriksson, C. Lu, P. Ödling, and P. O. Börjesson, "Enabling DSL and Radio on the Same Copper Pair," in *Proc. IEEE International Conference on Communications (ICC)*, 2015.

[5] T.-C. Lee and B. Razavi, "A 125-MHz mixed-signal echo canceller for Gigabit Ethernet on copper wire," *Solid-State Circuits, IEEE Journal of*, vol. 36, no. 3, pp. 366–373, March 2001.

[6] ITU-R, "Propagation data and prediction methods for the planning of indoor radiocommunication systems and radio local area networks in the frequency range 900 MHz to 100 GHz," International Telecommunication Union (ITU), Recommendation P.1238-7, February 2012. [Online]. Available: http://goo.gl/ZMIY7E

[7] 3GPP, "Evolved Universal Terrestrial Radio Access (E-UTRA); Base Station (BS) radio transmission and reception," 3rd Generation Partnership Project (3GPP), TS 36.104 V12.6.0, February 2015. [Online]. Available: http://goo.gl/SCislQ

[8] ——, "Evolved Universal Terrestrial Radio Access (E-UTRA); User Equipment (UE) radio transmission and reception," 3rd Generation Partnership Project (3GPP), TS 36.101 V12.5.0, November 2014. [Online]. Available: http://goo.gl/1PRPLV

[9] D. Acatauassu, S. Höst, C. Lu, M. Berg, A. Klautau, and P. O. Börjesson, "Simple and causal copper cable model suitable for g.fast frequencies," *IEEE Transactions on Communications*, vol. 62, no. 11, pp. 4040–4051, November 2014.

[10] Pulse, "Hybrid VDSL Transformer for Use with Infineon VDSL 2-Band, 4-Band and 10Base-S Chipsets," datasheet, 2003.